NASA TECHNICAL NOTE

NASA TN D-5801

NASA TN D-5801

A STABILITY STUDY AND MODAL ANALYSIS OF A SPACE-STATION—CENTRIFUGE CONFIGURATION

by Robert K. Sleeper and Harold C. Lester

Langley Research Center
Hampton, Va. 23365

NATIONAL AERONAUTICS AND SPACE ADMINISTRATION • WASHINGTON, D. C. • MAY 1970

1. Report No.	2. Government Accession No.	3. Rec...
NASA TN D-5801		

4. Title and Subtitle
A STABILITY STUDY AND MODAL ANALYSIS OF A SPACE-STATION—CENTRIFUGE CONFIGURATION

5. Report Date
May 1970

6. Performing Organization Code

7. Author(s)
Robert K. Sleeper and Harold C. Lester

8. Performing Organization Report No.
L-6597

9. Performing Organization Name and Address
NASA Langley Research Center
Hampton, Va. 23365

10. Work Unit No.
124-08-14-04-23

11. Contract or Grant No.

12. Sponsoring Agency Name and Address
National Aeronautics and Space Administration
Washington, D.C. 20546

13. Type of Report and Period Covered
Technical Note

14. Sponsoring Agency Code

15. Supplementary Notes

16. Abstract
The planar motion of a centrifuge—space-station configuration has been examined to determine the types of instabilities that can occur. Although the study is devoted primarily to undamped symmetric configurations, the effects on stability of linear viscous damping and mass asymmetry were also examined. A linear analysis which was effected by assuming constant speed rotation showed that with little or no damping, unstable motion can occur in rotational speed ranges or regions representing two types of instabilities: (1) The first region was bounded by upper and lower critical speeds and in this region the motion consisted of a self-excited pure divergence similar to that found for rotating shafts with elliptical cross sections. All configurations exhibited this type of instability which was attributed to the bidirectional dynamic properties of the centrifuge. (2) Special attention has been directed toward a second type of instability which may be overlooked in an analysis but which can occur at rotational speeds above the critical speed; it consists of a self-excited oscillatory divergence similar to that experienced by helicopter pylon-rotor configurations. Configurations with a heavy centrifuge hub or light gondolas were more likely to have this type of instability. For undamped models a superposition of the complex eigenvectors is employed to represent the various types of real motion in the rotating reference frame and a special stability technique applicable to even-power polynomials is used to determine stability boundaries.

17. Key Words (Suggested by Author(s))	18. Distribution Statement
Space-station—centrifuge modal analysis Space-station—centrifuge stability	Unclassified – Unlimited

19. Security Classif. (of this report)	20. Security Classif. (of this page)	21. No. of Pages	22. Price*
Unclassified	Unclassified	75	$3.00

*For sale by the Clearinghouse for Federal Scientific and Technical Information
Springfield, Virginia 22151

A STABILITY STUDY AND MODAL ANALYSIS OF A SPACE-STATION—CENTRIFUGE CONFIGURATION

By Robert K. Sleeper and Harold C. Lester
Langley Research Center

SUMMARY

The planar motion of a centrifuge—space-station configuration has been examined to determine the types of instabilities that can occur. Although the study is devoted primarily to undamped symmetric configurations, the effects on stability of linear viscous damping and mass asymmetry were also examined.

A linear analysis which was effected by assuming constant speed rotation showed that with little or no damping, unstable motion can occur in rotational speed ranges or regions representing two types of instabilities: (1) The first region was bounded by upper and lower critical speeds and in this region the motion consisted of a self-excited pure divergence similar to that found for rotating shafts with elliptical cross sections. All configurations exhibited this type of instability which was attributed to the bidirectional dynamic properties of the centrifuge. (2) Special attention has been directed toward a second type of instability which may be overlooked in an analysis but which can occur at rotational speeds above the critical speed; it consists of a self-excited oscillatory divergence similar to that experienced by helicopter pylon-rotor configurations. Configurations with a heavy centrifuge hub or light gondolas were more likely to have this type of instability.

For undamped models a superposition of the complex eigenvectors is employed to represent the various types of real motion in the rotating reference frame and a special stability technique applicable to even-power polynomials is used to determine stability boundaries.

INTRODUCTION

A space station with an onboard rotating mechanism such as a centrifuge may exhibit instabilities such as those that have occurred with pylon-rotor configurations on helicopters in contact with the ground. For such configurations two types of instabilities have been found.

One type of instability is similar to that exhibited by a rotating shaft with an elliptical cross section, the critical speeds of which occur in pairs corresponding to the two principal stiffnesses. (See ref. 1.) Within the speed range bounded by the two critical speeds, the motion diverges in a nonoscillatory manner. The instability is classified as "self-excited" by virtue of the fact that the destabilizing force or forces are functions of the displacement vector and its derivatives.

The helicopter analysis (refs. 2 and 3) also showed that a second type of instability characterized by an oscillatory divergent motion can occur at speeds above the critical-speed range. This instability is referred to as a "self-excited mechanical instability" in references 2 and 3; the term "flutter" which more usually denotes an aeroelastic phenomenon (ref. 4) has been used by others (ref. 5). With either of these instabilities, kinetic energy of rotation is transformed into elastic energy. The energy transfer may be very rapid and may result in a catastrophic increase in the amplitude of the associated elastic deformation.

In the present study, which represents an extension of a previous study (ref. 6), the stability characteristics of a space station with an onboard centrifuge rotating at constant speed are studied. The mathematical model includes linear viscous damping, but the effects of gravity have been neglected. Linear differential equations describing small motions in the plane of the centrifuge are derived and presented in a nondimensional form.

Linear stability techniques are applied to determine and classify the regions of self-excited instability as a function of angular rotational speed for various combinations of the nondimensional system parameters. Furthermore, an eigenvalue-eigenvector solution is formulated by using an equivalent matrix of first-order equations of motion. Because of the lack of matrix symmetry, the eigenvectors are, in general, complex and hence classical vibration modes in the normal sense are not obtained. (See refs. 7 and 8.) However, it is demonstrated that the motion of the system can be described in terms of the complete set of eigenvectors for an arbitrary initial state vector. A Meerov-Fuller stability criterion (ref. 9) has been adapted to the analysis of the undamped system; it enabled a rapid determination of the parameter value combinations yielding unstable configurations. Although the effects of damping and mass asymmetries are demonstrated, most of the study is devoted to the undamped-symmetric model.

SYMBOLS

$A_1(\Omega^*), A_2(\Omega^*), A_3(\Omega^*)$ coefficients of sixth-order stability polynomial (see eq. (17))

a_1, a_2 axial displacements of gondolas due to lateral deflections (see fig. 2)

C	coefficient of viscous damping for hub support
c_1, c_2	coefficient of viscous damping for centrifuge arms
E	first-order dynamic matrix (see eq. (5))
$\tilde{E}$	uncoupled first-order dynamic matrix for undamped symmetric configuration (see eq. (14))
I	identity matrix
$j = \sqrt{-1}$	
K	hub support stiffness
k_1, k_2	equivalent spring stiffness of centrifuge arms
L_1, L_2	lengths of centrifuge arms
M_c	total mass of centrifuge, $m_1 + m_2 + M_h$
M_h	mass of hub
M_s	mass of space station (without centrifuge)
m_1, m_2	gondola masses
p	nondimensional Laplace variable, $s/\omega_e = \sigma^* + j\omega^*$
p_i	characteristic roots of system
$q_1(\ ), q_2(\ )$	generalized coordinates associated with lateral modal displacements $\phi_1(\rho)$ and $\phi_2(\rho)$, respectively
s	Laplace variable, $\sigma + j\omega$
t	time
t_0	reference time

X,Y coordinate axes with origin at center of mass of composite system and which rotate with centrifuge (see fig. 2)

X_f,Y_f space-fixed (inertial) axes with origin at center of mass of composite system (see fig. 2)

$\overline{X}$ state vector of four degree-of-freedom representation

$\left.\begin{matrix}\bar{x}_1(\ ),\bar{x}_2(\ ),\bar{x}_3(\ ),\\ \bar{x}_4(\ ),\bar{x}_5(\ ),\bar{x}_6(\ ),\\ \bar{x}_7(\ ),\bar{x}_8(\ )\end{matrix}\right\}$ transformed components of state vector of four degree-of-freedom representation (see eqs. (2))

x_h,y_h displacement coordinates of centrifuge hub relative to space-station (less centrifuge) center of mass (see fig. 2)

$\bar{x}_h(\ ),\bar{y}_h(\ )$ transformed relative displacement coordinates of centrifuge hub

x_s,y_s displacement coordinates of space station (less centrifuge) from center of mass of composite system (see fig. 2)

$\hat{Y}$ general complex response, $\hat{Y}_o e^{p\tau}$

$\hat{Y}_o$ complex amplitude

$\overline{Z}(\ )$ redefined transformed state vector of four degree-of-freedom representation (see eq. (12))

$\left.\begin{matrix}\bar{z}_1(\ ),\bar{z}_2(\ ),\bar{z}_3(\ ),\\ \bar{z}_4(\ ),\bar{z}_5(\ ),\bar{z}_6(\ ),\\ \bar{z}_7(\ ),\bar{z}_8(\ )\end{matrix}\right\}$ components of transformed state vector (see eqs. (11))

α distance from hub of effective hinge of centrifuge arm normalized to the arm length (see eq. (C6))

α_1,α_2 distance from hub of effective hinge of centrifuge arms normalized to arm lengths, L_1 and L_2, respectively

β rotation coordinate of centrifuge relative to space station (see fig. 2)

Δ_1,Δ_2 axial modal displacement factor of gondola masses due to lateral deflection

ζ viscous damping ratio of hub support relative to space station

ζ_1,ζ_2 viscous damping ratio for centrifuge arms relative to hub

Λ diagonal eigenvalue matrix (see eq. (27))

θ angle that system rotates during a quarter cycle at the natural frequency (see fig. 8(b))

μ_1,μ_2 ratios of gondola mass to centrifuge mass (see eqs. (1))

μ_3 ratio of centrifuge mass to space-station mass (see eqs. (1))

σ real part of Laplace variable s

σ^* real part of nondimensional Laplace variable, $\frac{\sigma}{\omega_e}$

τ nondimensional time referred to upper critical speed, $\omega_e t$

τ_o reference nondimensional time, $\omega_e t_o$ (see fig. 8)

ϕ complex modal matrix (see eq. (27))

$\phi_1(\rho),\phi_2(\rho)$ assumed lateral mode shapes for centrifuge

Ω centrifuge rotational speed relative to space station

Ω^* nondimensional rotational speed, $\frac{\Omega}{\omega_e}$

Ω_b,Ω_d rotational speeds corresponding to lower and upper critical speeds, respectively (see fig. 7)

ω imaginary part of Laplace variable s

ω^* imaginary part of nondimensional Laplace variable, $\frac{\omega}{\omega_e}$

ω_1,ω_2 uncoupled gondola-arm natural frequencies $\sqrt{k_1/m_1}$, $\sqrt{k_2/m_2}$, respectively

ω_3 uncoupled rigid centrifuge-support natural frequency, $\sqrt{K/M_c}$

ω_1^*, ω_2^* nondimensional gondola-arm natural frequencies ω_1/ω_e, ω_2/ω_e, respectively

ω_3^* nondimensional centrifuge-support natural frequency ω_3/ω_e

ω_e upper critical speed (frequency), $\sqrt{K(M_c + M_s)/M_s M_c}$

$\omega_{n,i}$ coupled natural frequency of system, i = 1, 2, 3, 4

$\omega_{n,i}^*$ nondimensional natural frequency of composite system, i = 1, 2, 3, 4

$\omega_{z,2}^*$ uncoupled natural frequency of antisymmetric degree of freedom (see eq. (29))

Bars over symbols denote Laplace transformed variable.

Superscript T denotes transposed matrix.

ANALYSIS

In this section, a basic mathematical model of a centrifuge-equipped space station is described and the governing equations of motion are presented and discussed. The equations are nondimensionalized and reduced to an equivalent set of first-order equations which are summarized in matrix form. From this matrix form the eigenvalues and eigenvectors of the configuration can be easily obtained.

The present analysis is devoted mainly to an undamped symmetric configuration. By using a coordinate transformation and nulling a system mass parameter, the equations of motion may be partially uncoupled. From the resulting set of equations, limiting curves of the stability boundaries are obtained and interpreted. In addition, the response of the configuration is expressed for a given initial state in terms of the eigenvectors and the effect of damping and mass asymmetries has been included in the analysis.

A detailed derivation of the equations of motion is given in appendix A.

Mathematical Model

A schematic illustration of the space-station—centrifuge model is given in figure 1. The mass of the space station without the centrifuge is denoted by M_s. The centrifuge is represented by a hub (pivot) mass M_h and two cantilever beam-like arms upon which the gondola masses m_1 and m_2 are attached. The arms of the centrifuge are assumed

to be massless with bending stiffnesses of k_1 and k_2, respectively. The lengths of the respective centrifuge arms are denoted as L_1 and L_2.

Assumptions used in the analysis are as follows:

(1) Motion is planar.

(2) The space station is kinematically constrained from rotating.

(3) The centrifuge rotates at a constant angular velocity Ω. (This constraint permits linearization of the equations of motion; however, the angular momentum and energy of the system are no longer conserved.)

(4) Effects of gravitation have been neglected.

(5) Small motions are assumed.

(6) The hub mass M_h is isotropically spring mounted and isotropically damped relative to the space station with springs of stiffness K and damping C. Damping of the centrifuge arms relative to the hub are denoted by c_1 and c_2.

Of particular importance are the axial displacements at the ends of the arms which result from lateral deflections. (See appendix B.) This effect provides stiffening proportional to the square of the rotational speed Ω with significant effects on the stability of the system.

Equations of Motion

Equations of motion have been derived by the method of Lagrange in appendix A for a general configuration. Subsequently, the equations are reduced to a simpler form for application to the assumed model wherein they become a set of linear differential equations with constant coefficients. (See eqs. (A58).)

Coordinate system.- Motion is referred to a coordinate system X,Y which rotates at the same rate Ω as the centrifuge. (See fig. 2.) In this rotating frame, the center of mass of the space station mass M_S (without the centrifuge attached) is located relative to a fixed (inertial) frame X_f,Y_f by the coordinates x_s,y_s and the angular displacement Ωt. As indicated in appendix A, the constant rotational speed constraint imposes only an externally applied moment to the system; therefore, the origin of the X,Y and X_f,Y_f coordinate systems may be conveniently interpreted as being located at the center of mass of the composite system. Relative to the center of mass of the space station, the displacement of the hub mass M_h is denoted by the coordinates x_h,y_h and finally, the lateral deflections of the gondola masses are denoted as q_1 and q_2. The axial displacements which are directed toward the hub are given by a_1 and a_2.

Reference to equations (A58) of appendix A indicates that the last four equations (in coordinates x_h, y_h, q_1, and q_2 are independent of the coordinates x_s and y_s. Thus, although equations (A58a) and (A58b) are coupled to equations (A58c) to (A58f)), the stability of the configuration is determined by the characteristic behavior of the latter equations. Therefore, the analysis is concentrated on these relations; that is, equations (A58c) to (A58f).

The Laplace transform is applied to the equations, and to provide a more general development, the following nondimensional parameters are introduced into the equations:

$$
\left.
\begin{aligned}
p &= \frac{s}{\omega_e} \\
\Omega^* &= \frac{\Omega}{\omega_e} \\
M_c &= m_1 + m_2 + M_h \\
\mu_1 &= \frac{m_1}{M_c} \\
\mu_2 &= \frac{m_2}{M_c} \\
\mu_3 &= \frac{M_c}{M_c + M_s} \\
\omega_1^* &= \frac{\omega_1}{\omega_e} = \frac{\sqrt{k_1/m_1}}{\omega_e} = \sqrt{\frac{(1 - \mu_3)k_1}{\mu_1 K}} \\
\omega_2^* &= \frac{\omega_2}{\omega_e} = \frac{\sqrt{k_2/m_2}}{\omega_e} = \sqrt{\frac{(1 - \mu_3)k_2}{\mu_2 K}} \\
\omega_3^* &= \frac{\omega_3}{\omega_e} = \frac{\sqrt{K/M_c}}{\omega_e} = \sqrt{1 - \mu_3} \\
\omega_e &= \frac{\omega_3}{\sqrt{1 - \mu_3}} = \sqrt{\frac{K(M_c + M_s)}{M_c M_s}} \\
\zeta_1 &= \frac{c_1}{2m_1\omega_1} \\
\zeta_2 &= \frac{c_2}{2m_2\omega_2} \\
\zeta &= \frac{C}{2M_c\omega_3}
\end{aligned}
\right\} \qquad (1)
$$

In these relations it should be noted that spring constants k_1 and k_2 have been substituted for the effective lateral stiffness of the beams that are described in equations (A17) and the upper critical speed ω_e has been used as a normalizing factor. In order to facilitate an eigenvalue-eigenvector solution, the equations are written in first-order form by using the following definitions:

$$\left.\begin{aligned}
\bar{x}_1 &= p\bar{x}_h \\
\bar{x}_2 &= p\bar{y}_h \\
\bar{x}_3 &= p\bar{q}_1 \\
\bar{x}_4 &= p\bar{q}_2 \\
\bar{x}_5 &= \bar{x}_h \\
\bar{x}_6 &= \bar{y}_h \\
\bar{x}_7 &= \bar{q}_1 \\
\bar{x}_8 &= \bar{q}_2
\end{aligned}\right\} \tag{2}$$

where the bar symbol ($^-$) has been used to denote a Laplace transformed coordinate and p is the nondimensional Laplace operator. Thus using the relationships

$$\left.\begin{aligned}
\bar{x}_1 &= p\bar{x}_5 \\
\bar{x}_2 &= p\bar{x}_6 \\
\bar{x}_3 &= p\bar{x}_7 \\
\bar{x}_4 &= p\bar{x}_8
\end{aligned}\right\} \tag{3}$$

together with the previous definitions, equations (A58c) to (A58f) may be written in the form

$$(E + pI)\bar{X} = 0 \tag{4}$$

where E is given for the general case as

$$
E = \begin{bmatrix}
\frac{2\zeta}{(1-\mu_3)^{1/2}} & -2\Omega^* & -2\mu_1\Omega^* & 2\mu_2\Omega^* & 1-\Omega^{*2} & -\frac{2\zeta\Omega^*}{(1-\mu_3)^{1/2}} & 0 & 0 \\
2\Omega^* & \frac{2\zeta(1-\mu_1\mu_3-\mu_2\mu_3)}{(1-\mu_3)^{1/2}(1-\mu_1-\mu_2)} & -\frac{2\mu_1\zeta_1\omega_1^*}{1-\mu_1-\mu_2} & \frac{2\mu_2\zeta_2\omega_2^*}{1-\mu_1-\mu_2} & \frac{2\zeta_3\Omega^*(1-\mu_1\mu_3-\mu_2\mu_3)}{(1-\mu_3)^{1/2}(1-\mu_1-\mu_2)} & \frac{1-\mu_1\mu_3-\mu_2\mu_3}{1-\mu_1-\mu_2}-\Omega^{*2} & -\frac{\mu_1}{1-\mu_1-\mu_2}\left[\omega_1^2+\Delta_1\Omega^{*2}\left(L_1-\mu_1L_1+\mu_2L_2\right)\right] & \frac{\mu_2}{1-\mu_1-\mu_2}\left[\omega_2^2+\Delta_2\Omega^{*2}\left(L_2-\mu_2L_2+\mu_1L_1\right)\right] \\
0 & -\frac{2\zeta(1-\mu_3)^{1/2}}{1-\mu_1-\mu_2} & \frac{2(1-\mu_2)\zeta_1\omega_1^*}{1-\mu_1-\mu_2} & -\frac{2\mu_2\zeta_2\omega_2^*}{1-\mu_1-\mu_2} & -\frac{2\zeta(1-\mu_3)^{1/2}\Omega^*}{1-\mu_1-\mu_2} & -\frac{1-\mu_3}{1-\mu_1-\mu_2} & \frac{\omega_1^2(1-\mu_2)}{1-\mu_1-\mu_2}+\Omega^{*2}\left[\Delta_1L_1-1+\frac{\mu_2\Delta_1\left(L_2-\mu_2L_2+\mu_1L_1\right)}{1-\mu_1-\mu_2}\right] & -\left[\frac{\mu_2\omega_2^{*2}}{1-\mu_1-\mu_2}+\frac{\mu_2\Delta_2\Omega^{*2}\left(L_2-\mu_2L_2+\mu_1L_1\right)}{1-\mu_1-\mu_2}\right] \\
0 & \frac{2\zeta(1-\mu_3)^{1/2}}{1-\mu_1-\mu_2} & -\frac{2\mu_1\zeta_1\omega_1^*}{1-\mu_1-\mu_2} & \frac{2(1-\mu_1)\zeta_2\omega_2^*}{1-\mu_1-\mu_2} & \frac{2\zeta(1-\mu_3)^{1/2}\Omega^*}{1-\mu_1-\mu_2} & \frac{1-\mu_3}{1-\mu_1-\mu_2} & -\left[\frac{\mu_1\omega_1^{*2}}{1-\mu_1-\mu_2}+\frac{\mu_1\Delta_1\Omega^{*2}\left(L_1-\mu_1L_1+\mu_2L_2\right)}{1-\mu_1-\mu_2}\right] & \frac{\omega_2^{*2}(1-\mu_1)}{1-\mu_1-\mu_2}+\Omega^{*2}\left[\Delta_2L_2-1+\frac{\mu_1\Delta_2\left(L_1-\mu_1L_1+\mu_2L_2\right)}{1-\mu_1-\mu_2}\right] \\
-1 & 0 & 0 & 0 & 0 & 0 & 0 & 0 \\
0 & -1 & 0 & 0 & 0 & 0 & 0 & 0 \\
0 & 0 & -1 & 0 & 0 & 0 & 0 & 0 \\
0 & 0 & 0 & -1 & 0 & 0 & 0 & 0
\end{bmatrix} \tag{5}
$$

and I is the identity matrix and

$$\bar{X}^T = \left[\bar{x}_1, \bar{x}_2, \bar{x}_3, \bar{x}_4, \bar{x}_5, \bar{x}_6, \bar{x}_7, \bar{x}_8\right] \tag{6}$$

It should be noted that matrix equation (4) is in the form of a nonsymmetric eigenvalue problem, the nondimensional Laplace variable p being the eigenvalue parameter. Equation (4) represents eight first-order linear differential equations with constant coefficients.

Undamped symmetric configuration.- The undamped symmetric centrifuge is of special interest because by means of a coordinate transformation a partial uncoupling of the equations result thereby and provide a deeper insight into the stability characteristics of the configuration. In addition, as will be shown subsequently, mode shapes of undamped configurations may be conveniently displayed. The equations of motion for the undamped symmetric configuration may be obtained by specializing the nondimensional parameters of equations (1) and the coefficients of the E matrix in accordance with the following:

$$\left.\begin{aligned} m_1 &= m_2 \\ L_1 &= L_2 \\ k_1 &= k_2 \\ \zeta_1 &= \zeta_2 = \zeta = 0 \end{aligned}\right\} \tag{7}$$

One of the four degrees of freedom may now be uncoupled from the analysis by combining coordinates. This uncoupling may be done by recognizing that

$$p\left(\bar{x}_3 + \bar{x}_4\right) + \left[\omega_1^{*2} + \Omega^{*2}\left(L_1 \Delta_1 - 1\right)\right]\left(\bar{x}_7 + \bar{x}_8\right) = 0 \tag{8}$$

and

$$p\left(\bar{x}_7 + \bar{x}_8\right) - \left(\bar{x}_3 + \bar{x}_4\right) = 0 \tag{9}$$

Substituting equation (9) into equation (8) gives the uncoupled second-order equation of motion in the new composite coordinate $\bar{x}_7 + \bar{x}_8$

$$\left\{p^2 + \left[\omega_1^{*2} + \Omega^{*2}\left(L_1 \Delta_1 - 1\right)\right]\right\}\left(\bar{x}_7 + \bar{x}_8\right) = 0 \tag{10}$$

Equation (10) describes an antisymmetric motion of the centrifuge arms about the hub which is independent of the other degrees of freedom of the system. Since $L_1 \Delta_1 \geqq 1$ for the configuration (as indicated in appendix B), the quantity in the brackets is always positive. Thus, the motion of this composite degree of freedom is always stable for all rotational speeds Ω^* and may be disregarded when stability is considered.

To complete the uncoupling process, the composite coordinate $\bar{x}_7 - \bar{x}_8$ is formed which remains coupled to the $\bar{x}_5$ and $\bar{x}_6$ degrees of freedom.

The uncoupled form of equation (4) may now be formulated by using the following definitions:

$$\left.\begin{aligned}
\bar{z}_1 &= \bar{x}_1 = p\bar{z}_5 \\
\bar{z}_2 &= \bar{x}_2 = p\bar{z}_6 \\
\bar{z}_3 &= \bar{x}_3 - \bar{x}_4 = p\bar{z}_7 \\
\bar{z}_4 &= \bar{x}_3 + \bar{x}_4 = p\bar{z}_8 \\
\bar{z}_5 &= \bar{x}_5 \\
\bar{z}_6 &= \bar{x}_6 \\
\bar{z}_7 &= \bar{x}_7 - \bar{x}_8 \\
\bar{z}_8 &= \bar{x}_7 + \bar{x}_8
\end{aligned}\right\} \tag{11}$$

and

$$\bar{Z}^T = \left\lfloor \bar{z}_1, \bar{z}_2, \bar{z}_3, \bar{z}_4, \bar{z}_5, \bar{z}_6, \bar{z}_7, \bar{z}_8 \right\rfloor \tag{12}$$

Thus, the eigenvalue problem becomes

$$\left(\tilde{E} + pI\right)\bar{Z} = 0 \tag{13}$$

where $\tilde{E}$ is the uncoupled form of the previously defined E-matrix for an undamped symmetric configuration:

$$\tilde{E} = \begin{bmatrix}
0 & -2\Omega^* & -2\mu_1\Omega^* & 0 & 1-\Omega^{*2} & 0 & 0 & 0 \\
2\Omega^* & 0 & 0 & 0 & 0 & \frac{1-2\mu_1\mu_3}{1-2\mu_1} - \Omega^{*2} & -\frac{\mu_1}{1-2\mu_1}\left(\omega_1^{*2} + \Delta_1 L_1 \Omega^{*2}\right) & 0 \\
0 & 0 & 0 & 0 & 0 & -\frac{2(1-\mu_3)}{1-2\mu_1} & \frac{1}{1-2\mu_1}\left[\omega_1^{*2} + \Omega^{*2}(\Delta_1 L_1 - 1 + 2\mu_1)\right] & 0 \\
0 & 0 & 0 & 0 & 0 & 0 & 0 & \omega_1^{*2} + \Omega^{*2}(\Delta_1 L_1 - 1) \\
-1 & 0 & 0 & 0 & 0 & 0 & 0 & 0 \\
0 & -1 & 0 & 0 & 0 & 0 & 0 & 0 \\
0 & 0 & -1 & 0 & 0 & 0 & 0 & 0 \\
0 & 0 & 0 & -1 & 0 & 0 & 0 & 0
\end{bmatrix} \tag{14}$$

Attention will be focused on the three coupled degrees of freedom.

Characteristic Stability Equation

The characteristic stability equation for the complete configuration is obtained by setting the determinant of the coefficients of either equation (4) or equation (13) to zero, that is,

$$\left| E + pI \right| = 0 \tag{15}$$

$$\left| \tilde{E} + pI \right| = 0 \tag{16}$$

Thus, if a root of equation (15) or (16) has a positive real part, the system is unstable.

It should be noted that equations (15) and (16) have the same characteristic polynomial and roots; however, for the undamped symmetric configuration the polynomial of equation (10) which is stable may be readily factored from equation (16) and disregarded. Thus only the three coupled degrees of freedom need to be considered, that is, the unshaded portion of $\tilde{E}$. By taking the determinant of the remaining 6×6 terms of the $\tilde{E}$-matrix a sixth-order polynomial in terms of $\bar{z}_1$, $\bar{z}_2$, $\bar{z}_3$, $\bar{z}_5$, $\bar{z}_6$, and $\bar{z}_7$ results of the form

$$p^6 + A_1(\Omega^*)p^4 + A_2(\Omega^*)p^2 + A_3(\Omega^*) = 0 \tag{17}$$

The coefficients A_1, A_2, and A_3 of the polynomial are functions of the physical parameters describing the system as well as the nondimensional rotational speed Ω^*. Note that the polynomial only contains coefficients of even powers of p as is usual for nonrotating systems and roots occur symmetrically about both the real and imaginary axes.

A three-dimensional plot of the locus of the characteristic roots of a symmetric configuration in terms of the nondimensional Laplace variable p and rotational speed Ω^* is shown in figure 3. A modal response of the form $\hat{Y} = \hat{Y}_o e^{p\tau}$ has been implied where $\hat{Y}$ is the (complex) response, $\hat{Y}_o$ is a complex coefficient, and τ is a nondimensional time, $\tau = \omega_e t$. The additional dimension Ω^* has been included to illustrate the effect of rotational speed on the roots. Since complex roots occur in conjugate pairs, only the positive imaginary roots are shown. In general, roots for the undamped configuration are stable and have purely oscillatory characteristics; hence, the roots are on the $j\omega^*,\Omega^*$-plane where the imaginary part of p is ω^*, a nondimensionalized natural frequency of the system. In the analysis for the undamped configuration, it will be advantageous to examine the locus of the roots on the $j\omega^*,\Omega^*$-plane, that is, for $p = j\omega_n^*$. It should be noted that the natural frequencies ω_n are frequencies that would be experienced in the rotating system as opposed to frequencies observed for the system in a fixed reference.

A typical root as shown at (a) is identified as the lowest of the three (coupled) conventional natural frequencies which the system has without rotation. If the behavior of this frequency is noted while the rotational speed is increased, it goes to zero after which it increases and may coalesce with another root before increasing indefinitely. Except where the two roots coalesce and the lowest root reduces to zero the roots generally increase along the imaginary axis with increasing rotational speed. This trend is due to a stiffening effect derived from the centrifugal forces of the rotating system.

Two unstable regions have been illustrated in figure 3 and the positive* portion of the surface enclosed by roots which are not purely imaginary is shown shaded. The instability which occurs at the lower rotational speed Ω^* for roots in the region of (b), (c), and (d) has no frequency or oscillatory characteristics but a purely divergent behavior with real roots as illustrated on the σ^*,Ω^*-plane. This behavior occurs between the two critical speeds derived from the bidirectional properties of the system and hence has been termed a critical speed instability. A second instability identified by roots having purely complex values and characterized by an oscillatory divergent behavior may exist at still higher rotational speeds. It is analogous to the mechanical instability exhibited by helicopter pylon-rotor configurations. (See refs. 2 and 3.)

*Positive in the sense of having roots with positive real parts.

When the undamped nonsymmetrical configuration is analyzed, the characteristic polynomial remains even but the equations of motion do not uncouple in the previously described manner. Thus, the locus that was ignored in the symmetric analysis must be included on the root locus display of figure 3. In fact, this locus may add another oscillatory instability.

For a configuration where damping has been introduced the characteristic polynomial is no longer even but, in general, may have coefficients of odd powers in p also. Consequently, the root locus will not be symmetric about the imaginary axis.

The roots of the undamped system have been investigated by using two methods. The first method examines the root locus on the $j\omega^*,\Omega^*$-plane of figure 3 and is described in the next section. The second approach utilizes a stability criterion which is adapted for the even characteristic polynomial to describe unstable regions. The mechanics of the adaptation may be seen by noting that a complex or p-plane plot of figure 3 may be illustrated by figure 4(a). The same locus in the p^2-plane will appear as shown in figure 4(b). Therefore, since all stable roots on the p-plane for all anticipated ranges of Ω^* must be on the imaginary axis, all stable roots on the p^2-plane must lie on the negative real axis. The Meerov-Fuller criterion (ref. 9) determines when a root of a polynomial is not negative and real.

With the addition of damping to the system, the locus plot is no longer confined to the $j\omega^*,\Omega^*$-plane and neither of the preceding techniques is applicable. However, the conventional Routh criterion (for example, see ref. 10) is applicable to the configuration and has been used to establish unstable regions.

Method of Uncoupling

An interesting insight into the nature of the oscillatory instability and the conditions under which it occurs can be found by examining an uncoupled form of the stability determinant of a symmetric undamped configuration on the $j\omega^*,\Omega^*$-plane as has been done in reference 2. The uncoupled root loci form limiting curves which approach the coupled loci when the rotational speed Ω^* is large, and these uncoupled loci are shown by the heavy solid lines and curves in figure 5. In the figure, centrifuge loci corresponding to two different configurations denoted by type I and type II curves have been included and the heavy straight lines with slopes of ± 1 depict the upper half of the uncoupled hub loci.

To develop the equations of the loci, it is convenient to refer to the equations of motion in second-order form. The matrix formulation for the symmetric configuration in terms of $\bar{z}_5$, $\bar{z}_6$, and $\bar{z}_7$ is

$$\begin{bmatrix} p^2 + 1 - \Omega^{*2} & -2\Omega^* p & -2\mu_1 \Omega^* p \\ 2\Omega^* p & p^2 + \left(\frac{1 - 2\mu_1\mu_3}{1 - 2\mu_1} - \Omega^{*2}\right) & -\left(\frac{\mu_1}{1 - 2\mu_1}\right)\left(\omega_1^{*2} + L_1 \Delta_1 \Omega^{*2}\right) \\ 0 & -\frac{2(1 - \mu_3)}{1 - 2\mu_1} & p^2 + \left(\frac{1}{1 - 2\mu_1}\right)\left[\omega_1^{*2} + \Omega^{*2}\left(L_1 \Delta_1 + 2\mu_1 - 1\right)\right] \end{bmatrix} \begin{Bmatrix} \bar{z}_5 \\ \bar{z}_6 \\ \bar{z}_7 \end{Bmatrix} = 0 \qquad (18)$$

An uncoupled analysis may only consider diagonal terms of a dynamical matrix; however, because of the strong coupling of $\bar{x}_h$ and $\bar{y}_h$ through the Coriolis acceleration in this problem, these degrees of freedom must be considered coupled, that is, the off-diagonal terms $-2\Omega^* p$ and $2\Omega^* p$ of the matrix equation (18) must be included. Furthermore, the condition that $\mu_1 \to 0$ must be impressed on the upper left 2×2 submatrix. Thus, the uncoupled hub behavior is represented by

$$\left[p^2 + \left(1 - \Omega^{*2}\right)\right]^2 + 4\Omega^{*2} p^2 = 0 \qquad (19)$$

which reduces to

$$\frac{\omega_n}{\omega_e} = \pm(\Omega^* - 1), \quad \pm(\Omega^* + 1) \qquad (20)$$

on the $j\omega^*, \Omega^*$-plane where $p = j\frac{\omega_n}{\omega_e}$ and ω_n is the natural frequency. These equations correspond to straight lines at $\pm 45^\circ$ to the Ω^*-axis of figure 5. The centrifuge behavior is represented by a hyperbolic curve corresponding to the diagonal element of the $\bar{z}_7 = q_1 - q_2$ degree of freedom. Thus, the equation for this uncoupled locus is

$$p^2 + \frac{\Omega^{*2}}{1 - 2\mu_1}\left(L_1 \Delta_1 + 2\mu_1 - 1\right) + \frac{\omega_1^{*2}}{1 - 2\mu_1} = 0 \qquad (21)$$

The approximate coupled root behavior of the centrifuge interacting with the hub is shown dashed at points A, B, and C. When two uncoupled loci cross, the coupled root loci may coalesce in a manner similar to that shown by the dashed lines in the neighborhood of the intersection of the type I uncoupled centrifuge locus and the $\Omega^* - 1$ asymptote as indicated at point A of figure 5. On the other hand, the root locus may couple without coalescing as shown at B, or in the neighborhood of the intersection of the type II uncoupled centrifuge locus and the $\Omega^* + 1$ asymptote as, for example, at point C. An oscillatory divergent instability occurs when roots coalesce and no longer remain purely imaginary,

that is, become complex. No instability results however when the roots couple without coalescing.

It can be seen that when the limiting slope of a hyperbolic centrifuge locus for large values of Ω^* is unity or greater, that is, the uncoupled centrifuge locus resembles that shown for type II, no unstable crossings of the hyperbolic curve and the $\Omega^* - 1$ asymptote occur. The condition which eliminates the intersection may be found by examining equation (21) for large Ω, that is,

$$p^2 + \frac{\Omega^{*2}}{1 - 2\mu_1}\left(L_1 \Delta_1 + 2\mu_1 - 1\right) \approx 0 \tag{22}$$

and making the slope equal to or greater than unity. Therefore, the following relation must be true:

$$\frac{L_1 \Delta_1 + 2\mu_1 - 1}{1 - 2\mu_1} \geqq 1 \tag{23}$$

Thus, no oscillatory instabilities should exist for

$$\mu_1 \geqq \frac{2 - L_1 \Delta_1}{4} \tag{24}$$

A result similar to expression (24) was established in reference 2.

In terms of α which is introduced in appendix C (see eq. (C6)) as the proportion of the length that the distance of the effective hinge point of the centrifuge arm is from the hub, equation (24) becomes

$$\mu_1 \geqq \frac{1}{4}\frac{1 - 2\alpha_1}{1 - \alpha_1} \tag{25}$$

Thus, for a symmetric configuration having arms behaving as uniform beams, $\alpha = 1/6$ and oscillatory instabilities should be prevented when

$$\mu_1 \geqq 0.2 \tag{26}$$

Because of the intrinsic geometrical nature of the parameter α, it is used throughout the remainder of the paper in lieu of Δ.

Modal Representation

Since the equations of motion are linear with constant coefficients, it is possible to represent the motion of the system by a superposition of the eigenvectors. Of special interest is the undamped configuration which exhibits sustained oscillatory motion (imaginary eigenvalues) when it is rotated at a constant angular speed.

If the eigenvalues or roots previously found are ascertained to be distinct, eigenvectors which satisfy the equations of motion may readily be found. Since the $\tilde{E}$-matrix as given by equation (14) is real and nonsymmetric, the eigenvectors and eigenvalues of equation (13) may be real or may occur in complex conjugate pairs. As in reference 11, a general expression for the time history may be given, in terms of nondimensional time τ, as

$$\overline{Z}(\tau) = \phi e^{\Lambda\tau}\phi^{-1}\overline{Z}(0) \tag{27}$$

where ϕ is the modal matrix and $\overline{Z}(0)$ is the initial state vector in first-order notation, Λ constitutes a diagonal matrix consisting of the eigenvalues p_i of the system, and $e^{\Lambda\tau}$ is a diagonal matrix having elements $e^{p_i\tau}$. In general, the modal displacement will be complex so that conventional time-invariant mode shapes do not exist but since eigenvectors occur in complex conjugate pairs and, when superimposed, may yield a real response, the time history may be illustrated by real modes which change with time. (See ref. 12.) Thus, for the undamped rotating system, its general motion may be displayed with real motions composed of pairs of mode shapes phased in time a quarter of a cycle apart.

When damping is introduced, the motion, in general, cannot be represented with real modes. Therefore, no convenient display is available.

DISCUSSION OF RESULTS

In this section, results are presented for several space-station—centrifuge configurations in order to illustrate the types of instabilities discussed previously. Physical parameters of the system are varied with respect to a reference model.

Basic Model

Properties.- The basic model assumed for this study was an undamped symmetric configuration defined by the following nondimensional parameters:

$$\left.\begin{aligned} \mu_1 &= \mu_2 = 0.1 \\ \mu_3 &= 0.01 \\ \alpha_1 &= \alpha_2 = \frac{1}{6} \\ \omega_1^* &= \omega_2^* = 0.1 \end{aligned}\right\} \tag{28}$$

The α values have been assumed to be consistent with those of a uniform cantilevered beam under the influence of a tip load (eq. (C6)) and a stiffness ratio $\frac{k_1}{K} = \frac{k_2}{K} = 0.00101$ has been implied by the ω^* value.

Instability regions.- A plot of the natural frequencies ω_n^* of the basic model for rotational speeds Ω^* is shown in figure 6. The uncoupled antisymmetric mode (dashed curve) which has been neglected in the stability analysis is included for completeness. The faint broken lines denote the uncoupled loci of the degrees of freedom considered in the stability analysis which were introduced in figure 5. Thus, the basic model exhibits a type I centrifuge locus as classified in figure 5, and the frequency plot associated with the coupled degrees of freedom resembles that illustrated on the $j\omega^*,\Omega^*$-plane of figure 3.

Inasmuch as the loci corresponding to each degree of freedom of the system must be on the $j\omega^*,\Omega^*$-plane for stable operation and the system has four degrees of freedom, figure 6 shows two ranges of Ω^* for which the basic model is unstable. Points of identification a, b, d, e, and g of figure 3 are also shown in the figure. The region that is encountered at the lowest rotational speed occurs for a zero natural frequency in the rotating reference frame and extends from $\Omega^* = 0.725$ to $\Omega^* = 1$. (It should be noted that the upper boundary is unity because the axes have been normalized to the undamped upper critical speed.) The behavior of the degree of freedom in the region is characterized by a nonoscillatory or zero-frequency divergence. The two general displacement patterns for the critical speeds which bound the unstable region and occur as a result from the bidirectional properties of the configuration have been illustrated in figure 7. The various masses are indicated by circles of varying radii.

A second region where the locus is discontinuous occurs for $2.75 \leqq \Omega^* \leqq 4.22$ in figure 6. Unlike the first region, this unstable region is bounded by stable loci which possess frequency components. It follows that the unstable region as illustrated in figure 3, has an oscillatory divergent behavior. The motion, as suggested by the intersection of the uncoupled loci of figure 5, is derived from a coupling of the hub and centrifuge motions and is analogous to the self-excited mechanical instability experienced with helicopters (refs. 2 and 3). Although the usual configuration may, in general, preclude this instability, to ensure that its occurrence will not be a factor, the conditions under which it may occur have been emphasized in this work.

Mode shapes.- Further insight into the mechanics of the motion may be gained by examining the associated eigenvectors that characterized the motion for a particular value of Ω^*. As previously indicated, the associated eigenvectors are not necessarily real and, in general, are complex although they may be combined to represent a real motion. The motion may be interpreted as a combination of two conventional modes having common frequencies but with a quarter of a cycle phase difference. For example, a typical

combined eigenvector or "mode shape" may be graphically interpreted as shown in figure 8 where the undeformed schematic representation is shown in figure 8(a) for reference. The + symbol, it should be noted, indicates the center of mass of the system and all motion is referenced to the rotating X,Y frame as shown. One gondola is marked for identification and as previously denoted, the various masses are indicated by circles of varying radii.

Figure 8(b) shows a pair of displacement patterns indicative of a typical response in a mode which is derived from combining complex conjugate eigenvectors. The left-hand figure has been arbitrarily normalized to a unit gondola-to-hub deflection. The right-hand pattern occurs a quarter of a cycle later after the system has rotated counterclockwise through an angle θ. Nondimensional time $\tau = \omega_e t$ is indicated. Motions at other times than indicated are represented by superpositions of these modes. It should be pointed out that because of Coriolis acceleration, the hub and space-station traverse elliptic trajectories in a mode.

Before introducing the mode shapes for the three coupled degrees of freedom, the response of the uncoupled mode of equation (10) for an undamped symmetrical configuration is given. The natural frequency of the mode may be obtained from equation (10) as

$$\omega^*_{z,2} = \omega^*_{n,4} = \left(\omega^{*2}_1 + \Omega^{*2}\,\frac{\alpha_1}{1 - \alpha_1}\right)^{1/2} \tag{29}$$

where $p = j\omega^*_{z,2}$ has been assumed and the corresponding mode will have an antisymmetric deflection shape as shown in figure 9.

In order to identify the characteristic behavior of the remaining degrees of freedom, especially near an instability, mode shapes for the three coupled degrees of freedom have been computed and illustrated in figure 10 for selected (counterclockwise) rotational speeds. For each rotational speed Ω^*, the pairs of modes have been arranged with natural frequencies increasing from left to right. At $\Omega^* = 0$, the classical mode shapes which consist of two lateral motions and a longitudinal motion are shown. As the rotational speed is introduced, centrifugal accelerations couple the longitudinal and lateral motions (as shown by the mode shapes for $\Omega^* = 0.1$ and 0.7). The large angle θ at $\Omega^* = 0.7$ for the low frequency mode is indicative of the natural frequency approaching zero. Actually, at $\Omega^* = 0.725$ (fig. 6), the frequency ω^*_n becomes zero and has the nonoscillatory shape as illustrated in figure 7(a). When Ω^* equals 0.8 and 0.9 (fig. 10), the low frequency mode has split into two different modes, the eigenvector has become real, and the need to combine complex conjugate modes has been eliminated. The mode shown at the left is unstable (divergent) whereas its companion mode on the right is stable (convergent). Although the response of these modes changes in an exponential manner, it has no oscillatory nature. For $\Omega^* = 1.0$, the two modes combined to yield the critical

speed mode which was indicated in figure 7(b) and when $\Omega^* = 1.1$, the coupled-mode pair relationship which existed at rotational speeds Ω^* below the unstable region and for the other modes in the speed range discussed is reestablished.

For rotational speeds from $\Omega^* = 1.0$ to $\Omega^* = 2.7$, the system is stable and exhibits three modal pairs, but at $\Omega^* = 2.7$ as indicated by figure 6, the lower frequency modes approach a common frequency (and angle θ) and mode shape. For a slight increase in rotational speed, these modes couple and one mode which has been shown on the left exhibits the unstable behavior found in the oscillatory divergent instability region. As indicated, this motion exists for $2.75 \leqq \Omega^* \leqq 4.22$. The mode illustrated in the center, for the rotational speeds in this unstable region, is a companion of the unstable mode but it is stable. By noting the relative positions of the centrifuge and space station at $\Omega^* = 2.7$ and $\Omega^* = 4.3$, the figures show that the phasing of the interacting mode pairs is reversed as the rotational speed passes through the oscillatory instability region. At higher rotational speeds the motion is typical of stable motion.

Motions which are approached as the rotational speed becomes large (labeled $\Omega^* \rightarrow \infty$) have been included for completeness. The two higher natural frequencies approach the rotational speed frequency and the modal motion degenerates to pure rotation; this condition would be typical of the system if the centrifuge arms were rigid. The lower frequency never achieves the rotational speed frequency. Its motion remains oscillatory although the space station motion subsides and only lateral motion persists.

Effect on rotation.- The effect of rotation on the vibratory motion of the modes is to transform lineal oscillations normally experienced in an inertial system into motions having both an oscillatory and rotatory nature in the rotating reference frame. In this frame the basic motion describes an elliptic path and may traverse the path in a clockwise or counterclockwise sense. This relative motion has been called whirl in the literature (see, for example, ref. 2) and may be seen in the mode shape pairs in a reference frame that rotates with the centrifuge arms. For instance, when $\Omega^* = 0.1$, the hub or space station in the high-frequency mode traverses a path which is elliptical and opposed in direction to the counterclockwise direction of rotation of the centrifuge.

On the other hand, the intermediate frequency mode exhibits a counterclockwise whirl. On examining the whirl of the low-frequency mode, it is shown to vanish as the lower critical speed is approached and does not exist in the critical-speed instability region. Subsequently, the whirl sense reverses.

Symmetric Model Study

Several additional undamped symmetric configurations which represent variations from the basic model were investigated in order to ascertain the effects of parameter

changes on the stability and vibrational characteristics. Unless otherwise stated, parameters of the basic model have been assumed. (See eqs. (28).)

An operational space station may be designed with heavier gondolas or lighter hubs than those prescribed on the reference model. Thus, if the ratio of gondola mass to hub mass is made larger than 0.2, the oscillatory instability may be avoided. An analysis of a configuration which is the same as the basic model except that μ_1 is 0.3 has been conducted to investigate this case and to compare the behavior of the basic model with a configuration without the oscillatory instability. Figure 11 shows the frequency loci for the configuration. It should be noted that this configuration has a type II centrifuge locus as classified in figure 5. The critical speed range is slightly wider than that for the basic model; however, since the uncoupled loci of the centrifuge and hub do not cross as shown in region A of figure 5, this configuration is always stable for $\Omega^* > 1$. The only unstable speed range is $0.55 < \Omega^* < 1.0$ which is the critical-speed instability region.

Mode shapes for the configuration are shown in figure 12. They have been included to illustrate the interaction of the modes when there is no oscillatory instability. Above $\Omega^* = 1.0$, figure 12 does not display the concurrence of the modal pairs and frequencies which occurred for $\Omega^* = 2.7$ in figure 10 when the oscillatory instability was present. Instead, the interaction which occurs for the upper two frequency modes is stable and the two lower frequency modes approach hub modes similar to the upper two of figure 10 as Ω^* approaches ∞.

Effect of mass ratios.- A broader picture of the effects of the mass ratio μ_1 and stiffness ratio k_1/K on the instabilities of the basic model is shown in figure 13, where the Meerov-Fuller criterion adapted for undamped systems has been used. Note that for this approach, the centrifuge arms are assumed to have spring stiffnesses $k_1 = m_1\omega_1^2$ or $k_1/K = \mu_1\omega_1^{*2}/(1 - \mu_3)$. Figure 13(a) shows the effect of μ_1 and k_1/K on the critical-speed instability region. The ordinate displays the rotational speed normalized to the upper critical speed which at $\Omega^* = 1$ by virtue of the normalization, coincides with the upper bound of the unstable region for all μ_1. Since the lower critical speed is the lower bound of the instability region, the system is stable between the critical speeds and these regions are indicated for various values of μ_1. The figure shows that although small mass ratios μ_1 may reduce the instability region, small stiffness ratios tend to make the region larger. Thus, a larger stable region below the instability regions may be achieved for smaller μ_1 and larger k_1/K where the upper and lower critical speeds approach one another. It should be noted that these steps reduce the bidirectional or orthotropic characteristic of the centrifuge.

Figure 13(b) displays the effect of μ_1 and k_1/K on the higher speed instability region for three values of μ_1. The system is unstable within the indicated bands. As

previously indicated, no oscillatory instability exists for μ_1 equal to or greater than 0.2. Figure 13(b) shows that although increasing μ_1 (below $\mu_1 = 0.2$) tends to delay the instability to slightly higher Ω^* at small k_1/K, the regions occur at lower Ω^* for large k_1/K and they are wider for all k_1/K. Thus larger stable regions above the critical-speed instability region may be attained for $\mu_1 \geqq 0.2$ or when μ_1 is small and k_1/K is large.

The effect of μ_3 on the instability regions has not been displayed in the analysis since the system instabilities are relatively insensitive to this parameter in the ranges of interest. For $0 \geqq \mu_3 \geqq 0.2$, the instability regions changed insignificantly from that of the basic model although for μ_3 approaching 1, the instability regions were reduced.

Effect of hinge-distance ratio.- Another parameter which affects the stability in a manner similar to mass ratio μ_1 is the hinge distance ratio α_1 as given by equation (C6). The hinge distance may be changed by altering the stiffness distribution in the arms of the centrifuge. The effect of changing α_1 is illustrated in a plot showing the variation of normalized natural frequency ω^* with rotational speed Ω^*. Such a display is shown in figure 14 for the basic model having an effective hinge point closer to the hub, that is, for $\alpha_1 = 1/12$. Figure 14 resembles the plot for the basic model except that the oscillatory instability occurs at a lower speed and the critical-speed instability region is broader. Figure 15 shows that when $\alpha_1 = 1/3$, that is, the model hinge-point distance has been doubled, the natural-frequency variations show no oscillatory instability, and the critical-speed instability region is less. Indeed, as shown in the analysis, by a proper choice of μ_1 or α_1, the oscillatory instability may be eliminated. The outboard choice of hinge point, when it is feasible, appears to offer improved stable operating ranges.

Unsymmetrical Model Studies

By altering the relationships between μ_1 and μ_2, α_1 and α_2, or ω_1^* and ω_2^*, models which lack mass symmetry about the hub may be obtained. It should be noted, however, that mass balance, as reflected by equation (A57), was retained. In this study only mass asymmetries are considered which vary the natural frequencies as

$$\omega_2^* = \frac{\mu_2}{\mu_1}\,\omega_1^*$$

This relationship may be derived by assuming that both centrifuge arms are uniform beams with equal flexural rigidities.

Two unsymmetrical configurations were studied. The stability characteristics of the first configuration where the effective hinge distance of one arm α_1 has been halved from that of the other arm are shown in figure 16. Because of this change, a second

instability region at $\Omega^* = 1.5$ having an oscillatory divergent nature is introduced. Furthermore, figure 16 shows that the uncoupled mode no longer exists but becomes coupled into the system.

The second configuration may resemble a system having a centrifuge with a single gondola. For this model, μ_1 was halved (and ω_2^* doubled) and the natural frequencies are given in figure 17. The dynamic characteristics appear to be similar to those of figure 16 although in figure 17 the oscillatory instability regions are not as wide. Indeed the lower speed region is extremely narrow.

Thus, a general configuration may be conceived of having not only one but possibly two oscillatory-divergent instabilities whereby the condition of symmetry removes one of them. Since most actual configurations may have slight asymmetries, more than one oscillatory divergent instability region may be anticipated.

These studies on an undamped system indicate that unstable regions may occur for some rotating mechanisms such as the space-station centrifuge. Although the critical-speed instability might be anticipated, there is a second type of instability which could represent a dangerous operational condition and must be considered. Even though the instability always occurred at rotational speeds above the critical speeds, it has been shown that such an instability need not exist for an undamped system. In the next section an attempt is made to ascertain some effects of damping on the unstable regions.

Introduction of Damping

In an effort to ascertain trends that may be expected when an energy dissipation mechanism is added to the symmetric mathematical model, viscous dashpots were added between the gondola masses and the arms and between the hub and support structure (see eq. (A19)). The motivation for considering damping effects stems from the fact that damping can exert a destabilizing influence on systems which are nonconservative without damping (ref. 13). Thus, unstable regions for a series of damped configurations of the basic model were determined by using the general equations (5) and the Routh stability criterion. Hub damping values of $\zeta = 10^{-6}$, 0.01, 0.1, and 0.2 and gondola damping values of $\zeta_1 = \zeta_2 = 0.01$, 0.1, and 0.5 were inserted in the model, and stability was determined for a series of μ_1 and k_1/K ratios. Values of the critical damping ratio c_1/C may be obtained from the figure by using the following equation:

$$\frac{c_1}{C} = \frac{\zeta_1}{\zeta}\sqrt{\frac{\mu_1 k_1}{K}} \tag{30}$$

The studies conducted with equal nonzero gondola damping values $(\zeta_1 = \zeta_2)$ showed that gondola damping had no effect on the critical-speed instability. The hub damping

ratio ζ, however, had considerable influence on this instability. For example, with $\zeta = \zeta_1 = \zeta_2 = 0.01$, the frequency loci in the critical-speed region differed little from that shown in figure 13(a). However, increasing the hub damping ratio ζ resulted in considerable reduction in the purely divergent instability regions as shown in figure 18. As may be seen in this figure, this unstable region may be eliminated for proper combinations of gondola mass and stiffness ratio when adequate hub damping is present.

Furthermore, the results of the analysis indicate that both types of damping influence the oscillatory divergent instability region. For ζ_1/ζ large, as when $\zeta = 10^{-6}$ and $\zeta_1 = 0.01$ or 0.5, the stable regions above the critical-speed instability region were very small for all configurations with

$$0.01 \leqq \mu_1 \leqq 0.49$$

Equation (26) established a critical value of μ_1 above which the oscillatory instability ceased to exist for undamped configurations. However, since μ_1 for a symmetric configuration must be less than 0.5, this inequality indicates that for a damped configuration where ζ_1/ζ is large, no such limit exists.

Increasing ζ_1 results in an increased or decreased oscillatory divergent instability region. For example, consider the basic model with $\zeta = 0.01$. When $\zeta_1 = 0.01$, the unstable regions are reduced only slightly from the model with $\zeta = \zeta_1 = \zeta_2 = 0$, but when $\zeta_1 = \zeta_2 = 0.1$, closed oscillatory unstable regions were obtained as shown in figure 19. The unstable region when $\zeta_1 = 0.01$ has become insignificant in the ranges of stiffnesses and rotational speeds considered, and more configurations are shown to be stable. Although not shown, further reductions in unstable regions were found when the hub damping ratio ζ was increased to 0.1 and 0.2. Furthermore, the unstable bands of the undamped model shown in figure 13(b) for $\mu_1 = 0.05$ and 0.1 do not extend to higher stiffness ratios in figure 19, but generally encompass a larger range of rotational speeds for lower stiffness ratios. Figure 19 further shows that when $\mu_1 = 0.1$, there is a slight reduction in the Ω^* range of the unstable region as k_1/K approaches zero. This trend becomes much more predominant (fig. 20) when ζ_1 is increased to 0.5; as a result, there is an extension of the unstable regions over a wide range of rotational speeds and a narrow range of stiffness ratios. Of special interest is the appearance of the unstable region for $\zeta_1 = 0.2$ which did not exist for the model with less damping. Furthermore, this region represents a region which is isolated to a finite range of stiffness ratios. An additional value of μ_1, that is, $\mu_1 = 0.15$, has been included in the figure to indicate the increase in size of the unstable region which can occur as the $(\mu_1 = 0.2)$ critical value of μ_1 for the undamped model is approached.

RÉSUMÉ

A linear analysis has been conducted to determine the vibrational characteristics and stability boundaries of a centrifuge—space-station configuration. The mathematical model used in the analysis describes a centrifuge represented by two gondola masses and a hub mass, rotating at constant speed relative to a free but nonrotating space station. Massless beams which were cantilevered from the hub constituted the centrifuge arms and were assumed to support the centrifuge gondolas. The hub was attached to the space station by an isotropic spring. Planar motion was assumed and gravitational effects were neglected. Viscous damping was introduced into the centrifuge arms and support structure to study damping trends. Of special importance for stability considerations has been the inclusion of an axial component of motion for the gondolas resulting from lateral motion of the centrifuge arms. This secondary effect of the motion causes the natural frequency of the centrifuge arms to increase with rotational speed and is the source of a so-called centrifugal stiffening effect.

Equations of motion were derived by the method of Lagrange subject to two kinematical constraints: (1) the space station was constrained from rotating and (2) the centrifuge was constrained to rotate uniformly. The equations were referred to a coordinate frame which rotated uniformly with the centrifuge and which had its origin located at the center of mass of the composite system.

The resulting second-order differential equations were linearized by neglecting small nonlinear terms. These equations were nondimensionalized and reduced to an equivalent set of first-order equations and summarized in matrix form. Two analytical techniques were applied to determine the stability of the system. Stability of undamped configurations was studied by examining the natural frequencies at various rotational speeds. Instabilities using this technique were indicated by an absence of frequencies from the imaginary axis of a complex-plane plot of the roots. On the other hand, the effect of parameter changes on stability was demonstrated better by using stability criteria consisting of either an adaptation of the Meerov-Fuller criterion (for undamped systems) or the Routh criterion (for damped systems).

As in the case of the restrained helicopter, the study has shown that a centrifuge—space-station configuration can exhibit two types of instabilities. The instability which occurs at lower rotational speeds has been called a critical speed instability and has a nonoscillatory divergent characteristic in a reference frame rotating with the centrifuge. The higher speed instability was oscillatory divergent.

For symmetric configurations without damping, the critical speed instability, which was attributed to the bidirectional properties of the centrifuge, was found to exist for all configurations. By adjusting parameters to make the centrifuge characteristics less

directional, either by concentrating the centrifuge mass nearer the hub or by making the centrifuge arms stiff compared with the support stiffness, the region of instability could be reduced. Limited analyses indicated that this instability could also be alleviated by increasing the arm stiffness near the hub.

The oscillatory divergent instability may be attributed to the coupled motions of the centrifuge and hub degrees of freedom. Only a centrifuge having a ratio of gondola mass to hub mass less than a critical value exhibited this behavior and the range of unstable rotational speeds was largest for configurations near the critical parameter value. Larger critical values resulted when the region of the centrifuge arm nearest the hub was flexible. A second range of rotational speeds which exhibited the oscillatory instability existed for mass-balanced asymmetric configurations.

When viscous damping was introduced into the centrifuge arms and support structure of the model, both regions of instability were affected. Damping in the support structure reduced the critical speed instability and damping in the arms tended to stabilize certain systems operating at rotational speeds near an oscillatory instability. However, excessive damping in the arms had a destabilizing effect at higher rotational speeds.

Only configurations with a centrifuge constituting only a small fraction of the total space station mass were considered. Within this restriction, the dynamic behavior was found to be insensitive to variations of these masses.

Since the matrix form of the undamped model was nonsymmetric, the solutions possessed eigenvalues and eigenvectors which were either real or occurred in complex-conjugate pairs. A display of such modes of the model were presented. When the roots were complex (conjugate), the response appears as a dual mode exhibiting two interacting conventional modes. The complete set of eigenvectors was used in a general matrix expression for the time history of the resulting real motions.

Langley Research Center,
National Aeronautics and Space Administration,
Hampton, Va., March 9, 1970.

APPENDIX A

EQUATIONS OF MOTION

In this appendix, planar equations of motion for a general mathematical model of a centrifuge-equipped space station are derived and summarized in a reduced form. The equations are derived by the method of Lagrange subject to certain kinematical constraints.

Symbols

$a_1(\rho,t), a_2(\rho,t)$ axial displacements of centrifuge arms due to lateral deflections

C effective hub support viscous damping coefficient

D dissipation function

$EI_1(\rho), EI_2(\rho)$ flexural rigidity of centrifuge arms

I_o polar mass moment of inertia of space station (less centrifuge about its center of mass)

$\tilde{I}_1, \tilde{I}_2$ lateral modal mass unbalance about undeformed position (see eq. (A26))

$\bar{i}, \bar{j}$ unit vectors along the rotating coordinate axes X and Y, respectively

K effective hub support stiffness coefficient

L_1, L_2 lengths of centrifuge arms

M_1, M_2 total mass of centrifuge arms (including hub) (see eq. (A22))

M_c total mass of centrifuge, $M_1 + M_2 + M_h$

M_h mass of hub

M_s mass of space station

$m_1(\rho), m_2(\rho)$ distributed mass of centrifuge arms

APPENDIX A

m_1, m_2 mass of gondolas

$\tilde{m}_1, \tilde{m}_2$ generalized masses (see eq. (A16))

N_1, N_2 nonlinear terms (see eqs. (A36) and (A38))

N_{xs}, N_{ys} nonlinear terms (see eqs. (A30) and (A33))

Q_x generalized force associated with x generalized coordinate

$q_1(t), q_2(t)$ generalized coordinates associated with lateral mode shapes $\phi_1(\rho)$ and $\phi_2(\rho)$

$\overline{R}_1, \overline{R}_2$ position vectors locating arbitrary points on centrifuge

$\overline{R}_s$ position vector of space station center of mass (less centrifuge)

S_1, S_2 static mass unbalances of centrifuge about hub (see eqs. (A26))

T total kinetic energy of configuration

t time

$u_1(\rho,t), u_2(\rho,t)$ lateral deflection of centrifuge arms relative to undeformed position

V total potential energy of configuration

X,Y coordinate axes which rotate with centrifuge (see fig. 2)

X_f, Y_f space-fixed (inertial) axes (see fig. 2)

x arbitrary generalized coordinate (see eq. (A20))

$x_f( ), y_f( )$ coordinates along fixed (inertial) X_f, Y_f axes

x_h, y_h generalized coordinates of centrifuge hub relative to space station (see fig. 2)

x_s, y_s generalized coordinates of space station (less centrifuge) (see fig. 2)

APPENDIX A

β generalized coordinate of rotation of centrifuge relative to space station

$\gamma = \theta + \beta$

$\Delta_1(\rho),\Delta_2(\rho)$ axial modal displacement factors of centrifuge arms (see eqs. (A6))

$\delta(\rho)$ Dirac delta function

ζ_1,ζ_2 equivalent viscous damping ratios for centrifuge arms

θ generalized coordinate of rotation of space station relative to inertial space

λ dummy variable

ρ running coordinate along undeformed centrifuge arms originating at hub

$\phi_1(\rho),\phi_2(\rho)$ assumed lateral mode shapes for centrifuge (see eqs. (A1))

Ω centrifuge rotational speed relative to space station

ω_1,ω_2 uncoupled gondola-arm natural frequencies

Dots over symbols indicate time derivatives.

Mathematical Model

The space-station centrifuge model shown in figures 1 and 2 consists of a space-station mass denoted by M_S whose mass center is located relative to an inertial origin O by the generalized coordinates x_s,y_s measured along rotating axes X,Y with respect to the inertial axes x_f,y_f. The hub (center of rotation) of the centrifuge denoted by mass M_h is attached to the space station by linear springs and linear viscous dashpots, and the support structure is represented in a linear isotropic manner. The hub is located relative to the mass center of the space station by the generalized coordinates x_h,y_h. The arms of the centrifuge are represented by two massless beams cantilevered at the hub and supporting the gondola masses m_1 and m_2. The lateral deflections of the arms are approximated in terms of distributed coordinates as follows:

$$\left.\begin{aligned} u_1(\rho,t) &= \phi_1(\rho)\, q_1(t) \\ u_2(\rho,t) &= \phi_2(\rho)\, q_2(t) \end{aligned}\right\} \tag{A1}$$

where $q_1(t)$ and $q_2(t)$ are the generalized coordinates associated with the mode shapes. The quantities $\phi_1(\rho)$ and $\phi_2(\rho)$, respectively, of equations (A1) may be interpreted as approximating the lateral deflections of each centrifuge arm by a single term (the fundamental) in a modal series expansion.

Motion is allowed only in the plane of the centrifuge and the effects of gravitation are neglected. Initially, the formulation allows a rotational degree of freedom θ about the space-station center of mass and a rotational degree of freedom β representing an angular displacement of the centrifuge about its hub relative to the space station. Later, to make the equations amenable to analysis, the motion will be constrained in accordance with the following equations:

$$\left.\begin{aligned}\theta(t) &= 0\\ \beta(t) &= \Omega t\end{aligned}\right\} \tag{A2}$$

where Ω is a constant representing the steady spin rate of the centrifuge. The physical interpretation of equations (A2) is discussed in a subsequent section.

Energy Formulation

Vector relations.- In terms of the coordinate system (see figs. 1 and 2) which rotates with the centrifuge, the position vector $\bar{R}_S$ locating the center of gravity of the space-station mass M_S may be written as follows:

$$\bar{R}_S = x_S\bar{i} + y_S\bar{j} \tag{A3}$$

Similarly, the position vectors $\bar{R}_1$ and $\bar{R}_2$ locating an arbitrary point on the left and right arms (beams) of the centrifuge may be expressed as

$$\left.\begin{aligned}\bar{R}_1 &= \left[x_S + x_h + \rho - a_1(\rho,t)\right]\bar{i} + \left[y_S + y_h + u_1(\rho,t)\right]\bar{j}\\ \bar{R}_2 &= \left[x_S + x_h - \rho + a_2(\rho,t)\right]\bar{i} + \left[y_S + y_h - u_2(\rho,t)\right]\bar{j}\end{aligned}\right\} \tag{A4}$$

In equations (A4) ρ represents a running coordinate originating at the hub where it is positive in the sense of $\bar{i}$ for the right centrifuge arm and positive in the sense of $-\bar{i}$ for the left arm. The coordinates $u_1(\rho,t)$ and $u_2(\rho,t)$ represent the lateral deflections of the centrifuge arms and x_h,y_h locates the hub (center of rotation) of the centrifuge relative to the space station.

It should be noted that small axial displacements a_1 and a_2 have been included in the analysis which are representative of the inward displacement experienced by a

beam deflected laterally. An expression of this displacement for small lateral deflections may be expressed as follows (see p. 252 of ref. 14):

$$\left.\begin{aligned} a_1(\rho,t) &= \frac{1}{2}\int_0^{\rho}\left[\frac{du_1(\lambda,t)}{d\lambda}\right]^2 d\lambda \\ a_2(\rho,t) &= \frac{1}{2}\int_0^{\rho}\left[\frac{du_2(\lambda,t)}{d\lambda}\right]^2 d\lambda \end{aligned}\right\} \tag{A5}$$

where λ is a dummy variable replacing ρ. By using the assumption of equation (A1), this inward displacement (or shortening) may be expressed as

$$\left.\begin{aligned} a_1(\rho,t) &= \frac{1}{2}\Delta_1(\rho)\, q_1^2(t) \\ a_2(\rho,t) &= \frac{1}{2}\Delta_2(\rho)\, q_2^2(t) \end{aligned}\right\} \tag{A6}$$

where

$$\left.\begin{aligned} \Delta_1(\rho) &= \int_0^{\rho}\left[\frac{d\phi_1(\lambda)}{d\lambda}\right]^2 d\lambda \\ \Delta_2(\rho) &= \int_0^{\rho}\left[\frac{d\phi_2(\lambda)}{d\lambda}\right]^2 d\lambda \end{aligned}\right\} \tag{A7}$$

It should be noted that although $a_1(\rho,t)$ and $a_2(\rho,t)$ may be small, they provide a centrifugal stiffening term which has a significant effect on stability.

Equations (A3) and (A4) can be differentiated to give the velocity vectors which are required to determine the kinetic energy. In performing this differentiation, it must be noted that the unit vectors $\bar{i},\bar{j}$ are time dependent by virtue of the rotating reference frame. If γ is defined as

$$\gamma = \theta + \beta \tag{A8}$$

then it follows that

$$\left.\begin{aligned} \frac{d\bar{i}}{dt} &= \dot{\gamma}\bar{j} \\ \frac{d\bar{j}}{dt} &= -\dot{\gamma}\bar{i} \end{aligned}\right\} \tag{A9}$$

By using equations (A9) and taking the derivative of equation (A3), the velocity $\dot{\bar{R}}_s$ of the space station is given by

$$\dot{\bar{R}}_s = \left(\dot{x}_s - \dot{\gamma}y_s\right)\bar{i} + \left(\dot{y}_s + \dot{\gamma}x_s\right)\bar{j} \tag{A10}$$

and from equations (A4) with the use of equations (A9) the velocity of a point on the centrifuge becomes

$$\left.\begin{aligned}
\dot{\bar{R}}_1 &= \left\{\dot{x}_s + \dot{x}_h - \dot{a}_1(\rho,t) - \dot{\gamma}\left[y_s + y_h + u_1(\rho,t)\right]\right\}\bar{i} \\
&\quad + \left\{\dot{y}_s + \dot{y}_h + \dot{u}_1(\rho,t) + \dot{\gamma}\left[x_s + x_h + \rho - a_1(\rho,t)\right]\right\}\bar{j} \\
\dot{\bar{R}}_2 &= \left\{\dot{x}_s + \dot{x}_h + \dot{a}_2(\rho,t) - \dot{\gamma}\left[y_s + y_h - u_2(\rho,t)\right]\right\}\bar{i} \\
&\quad + \left\{\dot{y}_s + \dot{y}_h - \dot{u}_2(\rho,t) + \dot{\gamma}\left[x_s + x_h - \rho + a_2(\rho,t)\right]\right\}\bar{j}
\end{aligned}\right\} \tag{A11}$$

or

$$\left.\begin{aligned}
\dot{\bar{R}}_1 &= \left\{\dot{x}_s + \dot{x}_h - \Delta_1(\rho)\, q_1\dot{q}_1 - \dot{\gamma}\left[y_s + y_h + \phi_1(\rho)\, q_1\right]\right\}\bar{i} \\
&\quad + \left\{\dot{y}_s + \dot{y}_h + \phi_1(\rho)\,\dot{q}_1 + \dot{\gamma}\left[x_s + x_h + \rho - \tfrac{1}{2}\Delta_1(\rho)\, q_1^2\right]\right\}\bar{j} \\
\dot{\bar{R}}_2 &= \left\{\dot{x}_s + \dot{x}_h + \Delta_2(\rho)\, q_2\dot{q}_2 - \dot{\gamma}\left[y_s + y_h - \phi_2(\rho)\, q_2\right]\right\}\bar{i} \\
&\quad + \left\{\dot{y}_s + \dot{y}_h - \phi_2(\rho)\,\dot{q}_2 + \dot{\gamma}\left[x_s + x_h - \rho + \tfrac{1}{2}\Delta_2(\rho)\, q_2^2\right]\right\}\bar{j}
\end{aligned}\right\} \tag{A12}$$

when equations (A1) and (A6) are inserted. By using these relations (eqs. (A11) and (A12)) the complete kinetic energy of the configuration may readily be formulated.

Kinetic energy.- The kinetic energy of the configuration consists of the kinetic energy of the centrifuge and space station and may be written as

$$T = \frac{1}{2}M_s\left[\dot{x}_s^2 + \dot{y}_s^2 + \dot{\gamma}^2\left(x_s^2 + y_s^2\right) + 2\dot{\gamma}\left(x_s\dot{y}_s - y_s\dot{x}_s\right)\right]$$

$$+ \frac{1}{2}I_o\dot{\theta}^2 + \frac{1}{2}\int_0^{L_1}\dot{\bar{R}}_1 \cdot \dot{\bar{R}}_1\, m_1(\rho)\, d\rho + \frac{1}{2}\int_0^{L_2}\dot{\bar{R}}_2 \cdot \dot{\bar{R}}_2 m_2(\rho)\, d\rho \tag{A13}$$

where I_0 is the polar mass moment of inertia of the space station about its center of mass. Thus, when equations (A12) are substituted into equation (A13), the complete kinetic energy expression results.

Potential energy.- The potential energy V for the configuration consists of the strain energy due to the displacement of the centrifuge (hub) relative to the space station and the strain energy associated with lateral deflection (bending) of the centrifuge arms. In deriving an expression for the former, it may be convenient to reference the hub displacement to a nonrotating frame X,Y fixed in the space station and to use the equations for transformating the $\tilde{X},\tilde{Y}$ axes to the rotating axes, that is,

$$\left.\begin{aligned} \tilde{x}_h &= x_h \cos\gamma - y_h \sin\gamma \\ \tilde{y}_h &= x_h \sin\gamma + y_h \cos\gamma \end{aligned}\right\} \tag{A14}$$

to obtain the potential energy function for the configuration as given by

$$V = \frac{1}{2} K\left(x_h^2 + y_h^2\right) + \frac{1}{2} \tilde{m}_1 \omega_1^2 q_1^2(t) + \frac{1}{2} \tilde{m}_2 \omega_2^2 q_2^2(t) \tag{A15}$$

In equation (A15), the constant K is the equivalent isotropic spring constant for the centrifuge hub support structure. The other quantities are related to the mode shapes used in equations (A1) to describe the lateral deflections of the centrifuge arms. Specifically, the relations

$$\left.\begin{aligned} \tilde{m}_1 &= \int_0^{L_1} \phi_1^2(\rho)\, m_1(\rho)\, d\rho \\ \tilde{m}_2 &= \int_0^{L_1} \phi_2^2(\rho)\, m_2(\rho)\, d\rho \end{aligned}\right\} \tag{A16}$$

are the respective generalized masses associated with each mode shape and

$$\left.\begin{aligned} \omega_1^2 &= \frac{1}{\tilde{m}_1} \int_0^{L_1} (EI)_1 \left[\frac{d^2\phi_1(\rho)}{d\rho^2}\right]^2 d\rho \\ \omega_2^2 &= \frac{1}{\tilde{m}_2} \int_0^{L_2} (EI)_2 \left[\frac{d^2\phi_2(\rho)}{d\rho^2}\right]^2 d\rho \end{aligned}\right\} \tag{A17}$$

are the squares of the natural frequencies. (See ref. 4.)

APPENDIX A

Dissipation function.- In a manner similar to that used to derive the potential energy, the dissipation function D for the configuration may be initially expressed as

$$D = \frac{1}{2} C\left(\dot{\tilde{x}}_h^2 + \dot{\tilde{y}}_h^2\right) + \tilde{m}_1 \zeta_1 \omega_1 \dot{q}_1^2 + \tilde{m}_2 \zeta_2 \omega_2 \dot{q}_2^2 \tag{A18}$$

Then by using equations (A14) the dissipation function may be written in terms of quantities related to the rotating axes (see ref. 3):

$$D = \frac{1}{2} C\left[\dot{x}_h^2 + \dot{y}_h^2 + \dot{\gamma}^2\left(x_h^2 + y_h^2\right) + 2\dot{\gamma}\left(x_h \dot{y}_h - \dot{x}_h y_h\right)\right] + \tilde{m}_1 \zeta_1 \omega_1 \dot{q}_1^2 + \tilde{m}_2 \zeta_2 \omega_2 \dot{q}_2^2 \tag{A19}$$

where C is the viscous damping coefficient associated with the hub support structure and ζ_1 and ζ_2 are the equivalent viscous damping ratios associated with the respective arms of the centrifuge.

It should be noted that because of the homogeneous nature of the hub damping assumed for the model, the dissipation is expressed in terms of the total velocity of the hub relative to the space station which involves the rotational rate $\dot{\gamma}$.

Kinematical Constraints

Thus far the space-station—centrifuge configuration has been allowed eight degrees of freedom, namely: x_s, y_s, X_h, Y_h, q_1, q_2, θ, and β. It is at this stage of the development that the kinematical constraints given by equations (A2) are introduced into the formulation. This procedure may be accomplished by either explicitly defining the generalized forces (external) which maintain the constraints (Newtonian approach) or by implicitly accounting for the effect of these generalized forces by substituting the constraint conditions (eqs. (A2)) directly into the equations for the kinetic and potential energies and the dissipation function (method of analytical mechanics, ref. 15). The foundation for this latter approach which is used in the report utilizes Hamilton's principle and the calculus of variations. Thus, only the kinematical constraints need to be specified and not the generalized forces that maintain these constraints. It should be noted that with this approach the configuration possesses only six degrees of freedom, namely, x_s, y_s, X_h, Y_h, q_1, and q_2.

If the generalized forces which maintain the given kinematical constraints are of interest, they can be obtained by the method of Lagrange multipliers. (See ref. 15.) For the present situation this approach readily shows that the generalized force that maintains the constraint $\beta = \Omega t$ is a moment acting at the hub of the centrifuge and similarly that the constraint $\theta = 0$ is maintained by a moment acting on the space station.

Finally, since only external moments act on the configuration, linear momentum is conserved. The mass center of the configuration therefore remains fixed in space or translates with a constant velocity. Hence, the origin O of the space-fixed axes X_f, Y_f (see fig. 2) may be conveniently interpreted as being located at the center of mass of the configuration.

Lagrange's Equations of Motion

The equations of motion for the space-station—centrifuge configuration are derived by the method of Lagrange by substituting equations (A13), (A15), (A19), and $Q_x = 0$ into

$$\frac{d}{dt}\left(\frac{\partial T}{\partial \dot{x}}\right) - \frac{\partial T}{\partial x} + \frac{\partial V}{\partial x} + \frac{\partial D}{\partial \dot{x}} = Q_x \tag{A20}$$

where x represents an arbitrary generalized coordinate selected from the set $(x_S, y_S, x_h, y_h, q_1$, and $q_2)$. The technique is illustrated for the choice $x = x_S$. From equation (A13),

$$\frac{\partial T}{\partial \dot{x}_S} = M_S\left(\dot{x}_S - \dot{\gamma} y_S\right) + \int_0^{L_1} \dot{\bar{R}}_1 \cdot \frac{\partial \dot{\bar{R}}_1}{\partial \dot{x}_S} m_1(\rho)\, d\rho + \int_0^{L_2} \dot{\bar{R}}_2 \cdot \frac{\partial \dot{\bar{R}}_2}{\partial \dot{x}_S} m_2(\rho)\, d\rho \tag{A21}$$

and using the results of equations (A12) and defining the following integrals:

$$\left.\begin{aligned} M_1 &= \int_0^{L_1} m_1(\rho)\, d\rho \\ M_2 &= \int_0^{L_2} m_2(\rho)\, d\rho \end{aligned}\right\} \tag{A22}$$

equation (A21) reduces to

$$\begin{aligned} \frac{\partial T}{\partial \dot{x}_S} = {} & M_S\left(\dot{x}_S - \dot{\gamma} y_S\right) + M_1\left[\dot{x}_S + \dot{x}_h - \dot{\gamma}\left(y_S + y_h\right)\right] - q_1\dot{q}_1 \int_0^{L_1} \Delta_1(\rho)\, m_1(\rho)\, d\rho \\ & - \dot{\gamma} q_1 \int_0^{L_1} \phi_1(\rho)\, m_1(\rho)\, d\rho + M_2\left[\dot{x}_S + \dot{x}_h - \dot{\gamma}\left(y_S + y_h\right)\right] + q_2\dot{q}_2 \int_0^{L_2} \Delta_2(\rho)\, m_2(\rho)\, d\rho \\ & + \dot{\gamma} q_2 \int_0^{L_2} \phi_2(\rho)\, m_2(\rho)\, d\rho \end{aligned} \tag{A23}$$

APPENDIX A

Differentiating equation (A23) with respect to time produces

$$\frac{d}{dt}\left(\frac{\partial T}{\partial \dot{x}_S}\right) = M_S\left(\ddot{x}_S - \dot{\gamma}\dot{y}_S - \ddot{\gamma}y_S\right) + M_1\left[\ddot{x}_S + \ddot{x}_h - \ddot{\gamma}\left(y_S + y_h\right) - \dot{\gamma}\left(\dot{y}_S + \dot{y}_h\right)\right]$$

$$- \left(\dot{q}_1^2 + q_1\ddot{q}_1\right)\int_0^{L_1} \Delta_1(\rho)\, m_1(\rho)\, d\rho - \ddot{\gamma}q_1 \int_0^{L_1} \phi_1(\rho)\, m_1(\rho)\, d\rho$$

$$- \dot{\gamma}\dot{q}_1 \int_0^{L_1} \phi_1(\rho)\, m_1(\rho)\, d\rho + M_2\left[\ddot{x}_S + \ddot{x}_h - \ddot{\gamma}\left(y_S + y_h\right) - \dot{\gamma}\left(\dot{y}_S + \dot{y}_h\right)\right]$$

$$+ \left(\dot{q}_2^2 + q_2\ddot{q}_2\right)\int_0^{L_2} \Delta_2(\rho)\, m_2(\rho)\, d\rho + \ddot{\gamma}q_2 \int_0^{L_2} \phi_2(\rho)\, m_2(\rho)\, d\rho$$

$$+ \dot{\gamma}\dot{q}_2 \int_0^{L_2} \phi_2(\rho)\, m_2(\rho)\, d\rho \qquad \text{(A24)}$$

Next, differentiating the kinetic energy with respect to x_S gives

$$\frac{\partial T}{\partial x_S} = M_S\left(\dot{\gamma}^2 x_S + \dot{\gamma}\dot{y}_S\right) + M_1\dot{\gamma}\left[\dot{y}_S + \dot{y}_h + \dot{\gamma}\left(x_S + x_h\right)\right] + \tilde{I}_1\dot{\gamma}\dot{q}_1 + S_1\dot{\gamma}^2 - \frac{1}{2}\dot{\gamma}^2 q_1^2$$

$$\times \int_0^{L_1} \Delta_1(\rho)\, \phi_1(\rho)\, m_1(\rho)\, d\rho + M_2\dot{\gamma}\left[\dot{y}_S + \dot{y}_h + \dot{\gamma}\left(x_S + x_h\right)\right] - \tilde{I}_2\dot{\gamma}\dot{q}_2$$

$$- S_2\dot{\gamma}^2 + \frac{1}{2}\dot{\gamma}^2 q_2^2 \int_0^{L_2} \Delta_2(\rho)\, \phi_2(\rho)\, m_2(\rho)\, d\rho \qquad \text{(A25)}$$

where

$$\left.\begin{aligned} \tilde{I}_1 &= \int_0^{L_1} \phi_1(\rho)\, m_1(\rho)\, d\rho \qquad & S_1 &= \int_0^{L_1} \rho m_1(\rho)\, d\rho \\ \tilde{I}_2 &= \int_0^{L_2} \phi_2(\rho)\, m_2(\rho)\, d\rho \qquad & S_2 &= \int_0^{L_2} \rho m_2(\rho)\, d\rho \end{aligned}\right\} \qquad \text{(A26)}$$

APPENDIX A

From the potential energy function V as given by equation (A15) there is a contribution of

$$\frac{\partial V}{\partial x_S} = 0 \tag{A27}$$

and from the dissipation function D (eq. (A19)), there is a contribution of

$$\frac{\partial D}{\partial \dot{x}_S} = 0 \tag{A28}$$

Combining equations (A24), (A25), (A27), and (A28) in accordance with equation (A20) gives the Lagrangian equation of motion for the x_S degree of freedom (generalized coordinate) as follows:

For the x_S equation:

$$M_S\left(\ddot{x}_S - 2\Omega\dot{y}_S - \Omega^2 x_S\right) + \left(M_1 + M_2\right)\left[\ddot{x}_S + \ddot{x}_h - 2\Omega\left(\dot{y}_S + \dot{y}_h\right) - \Omega^2\left(x_S + x_h\right)\right]$$

$$- \left(S_1 - S_2\right)\Omega^2 - 2\Omega\tilde{I}_1\dot{q}_1 + 2\Omega\tilde{I}_2\dot{q}_2 = -N_{xs} \tag{A29}$$

where N_{xs} is composed of nonlinear terms as follows:

$$N_{xs} = -\left(\dot{q}_1^2 + q_1\ddot{q}_1\right)\int_0^{L_1} \Delta_1(\rho)\, m_1(\rho)\, d\rho + \left(\dot{q}_2^2 + q_2\ddot{q}_2\right)\int_0^{L_2} \Delta_2(\rho)\, m_2(\rho)\, d\rho$$

$$+ \frac{1}{2}\Omega^2 q_1^2 \int_0^{L_1} \Delta_1(\rho)\, \phi_1(\rho)\, m_1(\rho)\, d\rho - \frac{1}{2}\Omega^2 q_2^2 \int_0^{L_2} \Delta_2(\rho)\, \phi_2(\rho)\, m_2(\rho)\, d\rho \tag{A30}$$

In a similar manner, the equations of motion for the remaining degrees of freedom may be obtained and are:

For the x_h equation:

$$\left(M_1 + M_2\right)\left[\ddot{x}_S + \ddot{x}_h - 2\Omega\left(\dot{y}_S + \dot{y}_h\right) - \Omega^2\left(x_S + x_h\right)\right] - \left(S_1 - S_2\right)\Omega^2 - 2\Omega\tilde{I}_1\dot{q}_1$$

$$+ 2\Omega\tilde{I}_2\dot{q}_2 + C\left(\dot{x}_h - \Omega y_h\right) + Kx_h = -N_{xs} \tag{A31}$$

For the y_S equation:

$$M_S\left(\ddot{y}_S + 2\Omega\dot{x}_S - \Omega^2 y_S\right) + \left(M_1 + M_2\right)\left[\ddot{y}_S + \ddot{y}_h + 2\Omega\left(\dot{x}_S + \dot{x}_h\right) - \Omega^2\left(y_S + y_h\right)\right]$$

$$+ \tilde{I}_1\left(\ddot{q}_1 - \Omega^2 q_1\right) - \tilde{I}_2\left(\ddot{q}_2 - \Omega^2 q_2\right) = -N_{ys} \tag{A32}$$

where

$$N_{ys} = -2\Omega q_1\dot{q}_1 \int_0^{L_1} \Delta_1(\rho)\, m_1(\rho)\, d\rho + 2\Omega q_2\dot{q}_2 \int_0^{L_2} \Delta_2(\rho)\, m_2(\rho)\, d\rho \tag{A33}$$

For the y_h equation:

$$(M_1 + M_2)\left[\ddot{y}_s + \ddot{y}_h + 2\Omega(\dot{x}_s + \dot{x}_h) - \Omega^2(y_s + y_h)\right] + \tilde{I}_1(\ddot{q}_1 - \Omega^2 q_1) - \tilde{I}_2(\ddot{q}_2 - \Omega^2 q_2)$$

$$C(\dot{y}_h + \Omega x_h) + Ky_h = -N_{ys} \tag{A34}$$

For the q_1 equation:

$$\tilde{m}_1\ddot{q}_1 + 2\tilde{m}_1\zeta_1\omega_1\dot{q}_1 + \left[\tilde{m}_1\omega_1^2 - \tilde{m}_1\Omega^2 + \Omega^2 \int_0^{L_1} \rho\,\Delta_1(\rho)\, m_1(\rho)\, d\rho\right]q_1$$

$$+ \tilde{I}_1\left[\ddot{y}_s + \ddot{y}_h + 2\Omega(\dot{x}_s + \dot{x}_h) - \Omega^2(y_s + y_h)\right] - q_1\left[\ddot{x}_s + \ddot{x}_h - 2\Omega(\dot{y}_s + \dot{y}_h)\right.$$

$$\left. - \Omega^2(x_s + x_h)\right] \int_0^{L_1} \Delta_1(\rho)\, m_1(\rho)\, d\rho = -N_1 \tag{A35}$$

where

$$N_1 = \left(q_1\dot{q}_1^2 + q_1^2\ddot{q}_1 - \frac{1}{2}\Omega^2 q_1^3\right) \int_0^{L_1} \Delta_1^2(\rho)\, m_1(\rho)\, d\rho \tag{A36}$$

For the q_2 equation:

$$\tilde{m}_2\ddot{q}_2 + 2\tilde{m}_2\zeta_2\omega_2\dot{q}_2 + \left[\tilde{m}_2\omega_2^2 - m_2\Omega^2 + \Omega^2 \int_0^{L_2} \rho\,\Delta_2(\rho)\, m_2(\rho)\, d\rho\right]q_2$$

$$- \tilde{I}_2\left[\ddot{y}_s + \ddot{y}_h + 2\Omega(\dot{x}_s + \dot{x}_h) - \Omega^2(y_s + y_h)\right] + q_2\left[\ddot{x}_s + \ddot{x}_h\right.$$

$$\left. - 2\Omega(\dot{y}_s + \dot{y}_h) + \Omega^2(x_s + x_h)\right] \int_0^{L_2} \Delta_2(\rho)\, m_2(\rho)\, d\rho = -N_2 \tag{A37}$$

where

$$N_2 = \left(q_2\dot{q}_2^2 + q_2^2\ddot{q}_2 - \frac{1}{2}\Omega^2 q_2^3\right) \int_0^{L_2} \Delta_2^2(\rho)\, m_2(\rho)\, d\rho \tag{A38}$$

It should be noted that residual nonlinear terms in equations (A35) and (A37) are underlined and have purposely not been included in N_1 and N_2. It will be shown later that these residual nonlinear terms combine to produce a linear term proportional to Ω^2.

APPENDIX A

Reduction of the Equations

In reducing the equations of motion to a form more amenable to a linear stability analysis, the nonlinear terms N_{xs}, N_{ys}, N_1, and N_2 are assumed to be small. Furthermore, the centrifuge is assumed to consist of two massless arms with bending rigidities $(EI)_1$ and $(EI)_2$, a hub mass M_h, and two gondola masses m_1 and m_2 as shown in figures 1 and 2. The mass distributions reflecting these assumptions are given by

$$\left.\begin{aligned} m_1(\rho) &= \frac{1}{2} M_h \delta(\rho) + m_1 \delta(\rho - L_1) \qquad (0 \leq \rho \leq L_1) \\ m_2(\rho) &= \frac{1}{2} M_h \delta(\rho) + m_2 \delta(\rho - L_2) \qquad (0 \leq \rho \leq L_2) \end{aligned}\right\} \tag{A39}$$

where the Dirac delta function δ has been employed in the definition. In addition, the mode shapes are assumed to be normalized so that

$$\phi_1(L_1) = \phi_2(L_2) = 1 \tag{A40}$$

By use of equations (A39) and (A40), it now appears that

$$\left.\begin{aligned} M_1 &= \frac{1}{2} M_h + m_1 \\ M_2 &= \frac{1}{2} M_h + m_2 \\ S_1 &= m_1 L_1 \\ S_2 &= m_2 L_2 \\ \tilde{I}_1 &= m_1 \\ \tilde{I}_2 &= m_2 \\ \tilde{m}_1 &= m_1 \\ \tilde{m}_2 &= m_2 \\ \int_0^{L_1} \Delta_1(\rho)\, m_1(\rho)\, d\rho &= m_1 \Delta_1(L_1) \\ \int_0^{L_2} \Delta_2(\rho)\, m_2(\rho)\, d\rho &= m_2 \Delta_2(L_2) \end{aligned}\right\}$$

(Equations continued on next page)

APPENDIX A

$$\left.\begin{aligned}
&\int_0^{L_1} \rho\,\Delta_1(\rho)\, m_1(\rho)\, d\rho = m_1 L_1 \Delta_1(L_1) \\
&\int_0^{L_2} \rho\,\Delta_2(\rho)\, m_2(\rho)\, d\rho = m_2 L_2 \Delta_2(L_2) \\
&\int_0^{L_1} \phi_1(\rho)\,\Delta_1(\rho)\, m_1(\rho)\, d\rho = m_1 \Delta_1(L_1) \\
&\int_0^{L_2} \phi_2(\rho)\,\Delta_2(\rho)\, m_2(\rho)\, d\rho = m_2 \Delta_2(L_2)
\end{aligned}\right\} \qquad \text{(A41)}$$

By using equations (A41), the equations of motion may be summarized as follows:

For the x_s equation:

$$M_s\left(\ddot{x}_s - 2\Omega\dot{y}_s - \Omega^2 x_s\right) + \left(M_h + m_1 + m_2\right)\left[\ddot{x}_s + \ddot{x}_h - 2\Omega\left(\dot{y}_s + \dot{y}_h\right) - \Omega^2\left(x_s + x_h\right)\right]$$

$$- \left(m_1 L_1 - m_2 L_2\right)\Omega^2 - 2m_1\Omega\dot{q}_1 + 2m_2\Omega\dot{q}_2 = 0 \qquad \text{(A42)}$$

For the x_h equation:

$$\left(M_h + m_1 + m_2\right)\left[\ddot{x}_s + \ddot{x}_h - 2\Omega\left(\dot{y}_s + \dot{y}_h\right) - \Omega^2\left(x_s + x_h\right)\right] - \left(m_1 L_1 - m_2 L_2\right)\Omega^2$$

$$- 2m_1\Omega\dot{q}_1 + 2m_2\Omega\dot{q}_2 + C\left(\dot{x}_h - \Omega y_h\right) + Kx_h = 0 \qquad \text{(A43)}$$

For the y_s equation:

$$M_s\left(\ddot{y}_s + 2\Omega\dot{x}_s - \Omega^2 y_s\right) + \left(M_h + m_1 + m_2\right)\left[\ddot{y}_s + \ddot{y}_h + 2\Omega\left(\dot{x}_s + \dot{x}_h\right) - \Omega^2\left(y_s + y_h\right)\right]$$

$$+ m_1\left(\ddot{q}_1 - \Omega^2 q_1\right) - m_2\left(\ddot{q}_2 - \Omega^2 q_2\right) = 0 \qquad \text{(A44)}$$

For the y_h equation:

$$\left(M_h + m_1 + m_2\right)\left[\ddot{y}_s + \ddot{y}_h + 2\Omega\left(\dot{x}_s + \dot{x}_h\right) - \Omega^2\left(y_s + y_h\right) + m_1\left(\ddot{q}_1 - \Omega^2 q_1\right)\right]$$

$$- m_2\left(\ddot{q}_2 - \Omega^2 q_2\right) + C\left(\dot{y}_h + \Omega x_h\right) + Ky_h = 0 \qquad \text{(A45)}$$

APPENDIX A

For the q_1 equation:

$$m_1\ddot{q}_1 + 2m_1\rho_1\omega_1\dot{q}_1 + \left[m_1\left(\omega_1^2 - \Omega^2\right) + m_1L_1\Delta_1(L_1)\Omega^2\right]q_1 + m_1\left[\ddot{y}_s + \ddot{y}_h + 2\Omega\left(\dot{x}_s + \dot{x}_h\right) - \Omega^2\left(y_s + y_h\right)\right] - m_1\Delta_1(L_1)\left[\ddot{x}_s + \ddot{x}_h - 2\Omega\left(\dot{y}_s + \dot{y}_h\right) - \Omega^2\left(x_s + x_h\right)\right]q_1 = 0 \tag{A46}$$

For the q_2 equation:

$$m_2\ddot{q}_2 + 2m_2\rho_2\omega_2\dot{q}_2 + \left[m_2\left(\omega_2^2 - \Omega^2\right) + m_2L_2\Delta_2(L_2)\Omega^2\right]q_2 - m_2\left[\ddot{y}_s + \ddot{y}_h + 2\Omega\left(\dot{x}_s + \dot{x}_h\right) - \Omega^2\left(y_s + y_h\right)\right] + m_2\Delta_2(L_2)\left[\ddot{x}_s + \ddot{x}_h - 2\Omega\left(\dot{y}_s + \dot{y}_h\right) + \Omega^2\left(x_s + x_h\right)\right]q_2 = 0 \tag{A47}$$

The acceleration coupling found in these equations may be removed by combining equations (A42) to (A47); for example, subtracting equation (A43) from (A42) and defining

$$M_c = M_h + m_1 + m_2 \tag{A48}$$

gives the following for the x_s equation:

$$M_s\left(\ddot{x}_s - 2\Omega\dot{y}_s - \Omega^2x_s\right) - C\left(\dot{x}_h - \Omega y_h\right) - Kx_h = 0 \tag{A49}$$

In a similar manner, subtracting equation (A45) from (A44) gives for the y_s equation:

$$M_s\left(\ddot{y}_s + 2\Omega\dot{x}_s - \Omega^2y_s\right) - C\left(\dot{y}_h + \Omega x_h\right) - Ky_h = 0 \tag{A50}$$

In order to simplify the q_1 equation, equations (A43) and (A45) are used to eliminate the terms $\left[\ddot{x}_s + \ddot{x}_h - 2\Omega\left(\dot{y}_s + \dot{y}_h\right) - \Omega^2\left(x_s + x_h\right)\right]$ and $\left[\ddot{y}_s + \ddot{y}_h + 2\Omega\left(\dot{x}_s + \dot{x}_h\right) - \Omega^2\left(y_s + y_h\right)\right]$, respectively, from equation (A46) to obtain

$$m_1\left(M_h + m_2\right)\ddot{q}_1 + 2m_1M_c\zeta_1\omega_1\dot{q}_1 + \left[m_1M_c\omega_1^2 - m_1\left(M_h + m_2\right)\Omega^2 + m_1M_cL_1\Delta_1(L_1)\Omega^2 - m_1\Delta_1(L_1)\left(m_1L_1 - m_2L_2\right)\Omega^2\right]q_1 + m_1m_2\left(\ddot{q}_2 - \Omega^2q_2\right) - m_1C\left(\dot{y}_h + \Omega x_h\right) - m_1Ky_h = 0 \tag{A51}$$

In a similar manner, equation (A47) may be put in the following form:

$$m_2(M_h + m_1)\ddot{q}_2 + 2m_2M_c\zeta_2\omega_2\dot{q}_2 + \Big[m_2M_c\omega_2^2 - m_2(M_h + m_1)\Omega^2 + m_2M_cL_2\Delta_2(L_2)\Omega^2$$

$$- m_2\Delta_2(L_2)(m_1L_1 - m_2L_2)\Omega^2\Big]q_2 + m_1m_2(\ddot{q}_1 - \Omega^2q_1) + m_2C(\dot{y}_h + \Omega x_h) + m_2Ky_h = 0 \qquad (A52)$$

It should be noted that in performing the operations to obtain equations (A51) and (A52), the residual nonlinear terms have been retained with linear terms proportional to Ω^2.

Solving for $\ddot{q}_2$ in equation (A52) and substituting the resulting expression into equation (A51) gives the q_1 equation:

$$m_1M_hM_c\ddot{q}_1 + 2m_1M_c(M_h + m_1)\zeta_1\omega_1\dot{q}_1 + \Big[m_1M_c(M_h + m_1)\omega_1^2 - m_1M_hM_c\Omega^2$$

$$+ m_1M_c(M_h + m_1)L_1\Delta_1(L_1)\Omega^2 - m_1(M_h + m_1)\Delta_1(L_1)(m_1L_1 - m_2L_2)\Omega^2\Big]q_1$$

$$- 2m_1m_2M_c\zeta_2\omega_2\dot{q}_2 - \Big[m_1m_2M_c\omega_2^2 + m_1m_2M_cL_2\Delta_2(L_2)\Omega^2$$

$$- m_1m_2\Delta_2(L_2)(m_1L_1 - m_2L_2)\Omega^2\Big]q_2 - m_1M_cC(\dot{y}_h + \Omega x_h) - m_1M_cKy_h = 0 \qquad (A53)$$

Solving for $\ddot{q}_1$ from equation (A51) and substituting the resulting expression into equation (A52) gives the q_2 equation:

$$m_2M_hM_c\ddot{q}_2 + 2m_2M_c(M_h + m_2)\zeta_2\omega_2\dot{q}_2 + \Big[m_2M_c(M_h + m_2)\omega_2^2 - m_2M_hM_c\Omega^2$$

$$+ m_2M_c(M_h + m_2)L_2\Delta_2(L_2)\Omega^2 - m_2(M_h + m_2)\Delta_2(L_2)(m_1L_1 - m_2L_2)\Omega^2\Big]q_2$$

$$- 2m_1m_2M_c\zeta_1\omega_1\dot{q}_1 - \Big[m_1m_2M_c\omega_1^2 + m_1m_2M_cL_1\Delta_1(L_1)\Omega^2$$

$$- m_1m_2\Delta_1(L_1)(m_1L_1 - m_2L_2)\Omega^2\Big]q_1 + m_2M_cC(\dot{y}_h + \Omega x_h) + m_2M_cKy_h = 0 \qquad (A54)$$

By using the results of equation (A49), equation (A43) can be written as the x_h equation:

$$M_cM_s(\ddot{x}_h - 2\Omega\dot{y}_h - \Omega^2x_h) + M_s(m_1L_1 - m_2L_2)\Omega^2 - 2m_1M_s\Omega\dot{q}_1 + 2m_2M_s\Omega\dot{q}_2$$

$$+ (M_s + M_c)C(\dot{x}_h - \Omega y_h) + (M_s + M_c)Kx_h = 0 \qquad (A55)$$

It should be noted that this equation contains a steady internally applied force proportional to Ω^2 which disappears when the centrifuge is balanced, that is, $m_1L_1 = m_2L_2$ and by using equations (A50), (A53), and (A54), equation (A45) can be expressed as follows:

$$M_cM_hM_s\left(\ddot{y}_h + 2\Omega\dot{x}_h - \Omega^2y_h\right) - 2m_1M_cM_s\zeta_1\omega_1\dot{q}_1 - \left[m_1M_cM_s\omega_1^2 + m_1M_cM_sL_1\Delta_1(L_1)\Omega^2\right.$$

$$\left. - m_1M_s\Delta_1(L_1)\left(m_1L_1 - m_2L_2\right)\Omega^2\right]q_1 + 2m_2M_cM_s\zeta_2\omega_2\dot{q}_2 + \left[m_2M_cM_s\omega_2^2\right.$$

$$\left. + m_2M_cM_sL_2\Delta_2(L_2)\Omega^2 - m_2M_s\Delta_2(L_2)\left(m_1L_1 - m_2L_2\right)\Omega^2\right]q_2 + M_c\left(M_s + M_h\right)C\left(\dot{y}_h + \Omega x_h\right)$$

$$+ M_c\left(M_s + M_h\right)Ky_h = 0 \qquad \text{(A56)}$$

Equations (A49), (A50), (A53), (A54), (A55), and (A56) represent the governing equations of motion for the configuration and are summarized in the following section subject to the restriction that $m_1L_1 - m_2L_2 = 0$.

Summary of Reduced Equations

It should be recalled that in developing the equations of motion, the centrifuge was constrained to rotate at a constant angular velocity Ω relative to the space station. The space station was assumed to be constrained against rotational motion. In addition, nonlinear terms were neglected. In summarizing the final dimensional form of the equations of motion, one additional assumption is made, that is, it is assumed that the centrifuge in the undeformed state is statically balanced about the hub as defined by the following equation:

$$m_1L_1 - m_2L_2 = 0 \qquad \text{(A57)}$$

The equations of motion may now be summarized as follows:

$$\ddot{x}_s - 2\Omega\dot{y}_s - \Omega^2x_s - \frac{C}{M_s}\left(\dot{x}_h - \Omega y_h\right) - \frac{K}{M_s}x_h = 0 \qquad \text{(A58a)}$$

$$\ddot{y}_s + 2\Omega\dot{x}_s - \Omega^2y_s - \frac{C}{M_s}\left(\dot{y}_h + \Omega x_h\right) - \frac{K}{M_s}y_h = 0 \qquad \text{(A58b)}$$

$$\ddot{x}_h - 2\Omega\dot{y}_h - \Omega^2x_h + \frac{M_s + M_c}{M_sM_c}C\left(\dot{x}_h - \Omega y_h\right) + \frac{M_s + M_c}{M_sM_c}Kx_h - \frac{2m_1\Omega}{M_c}\dot{q}_1 + \frac{2m_2\Omega}{M_c}\dot{q}_2 = 0 \qquad \text{(A58c)}$$

$$\ddot{y}_h + 2\Omega\dot{x}_h - \Omega^2 y_h + \frac{M_s + M_h}{M_s M_h} C\left(\dot{y}_h + \Omega x_h\right) + \frac{M_s + M_h}{M_s M_h} K y_h - \frac{2m_1\zeta_1\omega_1}{M_h}\dot{q}_1$$

$$- \left[\frac{m_1\omega_1^2}{M_h} + \frac{m_1 L_1 \Delta_1(L_1)\Omega^2}{M_h}\right] q_1 + \frac{2m_2\zeta_2\omega_2}{M_h}\dot{q}_2 + \left[\frac{m_2\omega_2^2}{M_h} + \frac{m_2 L_2 \Delta_2(L_2)\Omega^2}{M_h}\right] q_2 = 0 \qquad \text{(A58d)}$$

$$\ddot{q}_1 + \frac{2(M_h + m_1)\zeta_1\omega_1}{M_h}\dot{q}_1 + \left[\frac{(M_h + m_1)\omega_1^2}{M_h} - \Omega^2 + \frac{(M_h + m_1)L_1\Delta_1(L_1)\Omega^2}{M_h}\right] q_1$$

$$- \frac{2m_2\zeta_2\omega_2}{M_h}\dot{q}_2 - \left[\frac{m_2\omega_2^2}{M_h} + \frac{m_2 L_2 \Delta_2(L_2)\Omega^2}{M_h}\right] q_2 - \frac{C}{M_h}\left(\dot{y}_h + \Omega x_h\right) - \frac{K}{M_h} y_h = 0 \qquad \text{(A58e)}$$

$$\ddot{q}_2 + \frac{2(M_h + m_2)\zeta_2\omega_2}{M_h}\dot{q}_2 + \left[\frac{(M_h + m_2)\omega_2^2}{M_h} - \Omega^2 + \frac{(M_h + m_2)L_2\Delta_2(L_2)\Omega^2}{M_h}\right] q_2$$

$$- \frac{2m_1\zeta_1\omega_1}{M_h}\dot{q}_1 - \left[\frac{m_1\omega_1^2}{M_h} + \frac{m_1 L_1 \Delta_1(L_1)\Omega^2}{M_h}\right] q_1 + \frac{C}{M_h}\left(\dot{y}_h + \Omega x_h\right) + \frac{K}{M_h} y_h = 0 \qquad \text{(A58f)}$$

APPENDIX B

CENTRIFUGAL STIFFENING EFFECT

In this appendix the equation of motion for the forced response of a rotating cantilever beam is derived. The lateral deflection is approximated by a single term in a modal-form expansion. The resulting equation of motion is shown to contain a term proportional to the square of the rotational rate which includes the centrifugal stiffening effect. The tip of the cantilever beam is shown to follow a parabolic path.

Symbols

$a(x,t)$	axial shortening, equation (B1)
$EI(x)$	bending stiffness
$f(x,t)$	distributive loading
L	length of beam
M	generalized mass, equations (B4)
m	concentrated tip mass
$m(x)$	distributive mass
$Q(t)$	generalized force, equations (B4)
$q(\ )$	generalized coordinate, equation (B2)
t	time
X,Y	rotating reference frame
x	coordinates along X-axis
$u(x,t)$	lateral deflection parallel to Y-axis
λ	dummy variable for x

APPENDIX B

$\Delta(x)$ defined in equations (B4)

$\delta(x - L)$ Dirac delta function at $x = L$

$\phi(x)$ assumed mode shape

Ω rotational rate of beam

ω natural frequency of nonrotating beam (eqs. (B4))

ω_n natural frequency of rotating beam (eq. (B14))

A dot over a variable indicates differentiation with respect to time.

A prime over a variable indicates differentiation with respect to x.

Analysis of Centrifugal Stiffening

Consider the rotating centilever beam as shown in sketch (a) where Ω is the angular rate of rotation.

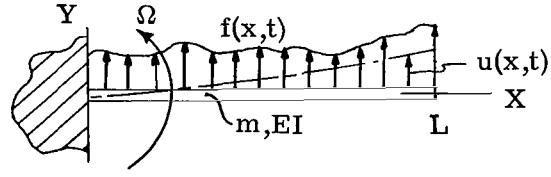

Sketch (a)

For any station x and time t there is an axial shortening $a(x,t)$ due to a lateral deflection $u(x,t)$. Thus, a point at coordinate x in the undeformed state is shifted toward the origin by the amount $a(x,t)$ where

$$a(x,t) = \frac{1}{2}\int_0^x u'^2(\lambda,t)\, d\lambda \tag{B1}$$

If Lagrange's equation for this system is used and a single term in a modal form expansion for the deflection $u(x,t)$ is assumed, that is

$$u(x,t) = \phi(x)\, q(t) \tag{B2}$$

the resulting equation of motion, the higher order nonlinear terms being neglected, is as follows:

$$M\ddot{q} + \left[M\left(\omega^2 - \Omega^2\right) + \Omega^2 \int_0^L xm(x)\, \Delta(x)\, dx\right] q = Q(t) \tag{B3}$$

where

$$\left.\begin{aligned} M &= \int_0^L \phi^2(x)\, m(x)\, dx \\ Q(t) &= \int_0^L f(x,t)\, \phi(x)\, dx \\ \omega^2 &= \frac{1}{M}\int_0^L EI\left[\phi''(x)\right]^2 dx \\ \Delta(x) &= \int_0^x \left[\phi'(\lambda)\right]^2 d\lambda \end{aligned}\right\} \tag{B4}$$

Equation (B3) is a forced undamped form of equation (A58e) of appendix A for a fixed hub support. Note that by the use of equation (B2) and the last relation of equations (B4), equation (B1) can be written as

$$a(x,t) = \frac{1}{2}\Delta(x)\, q^2(t) \tag{B5}$$

For the beam with a concentrated tip mass, that is,

$$m(x) = m\delta(x - L) \tag{B6}$$

where $\delta(x - L)$ is the Dirac delta function, equation (B3) becomes

$$\ddot{q} + \left\{\omega^2 + \Omega^2\left[L\,\Delta(L) - 1\right]\right\} q = Q(t) \tag{B7}$$

where

$$\Delta(L) = \int_0^L \left[\phi'(\lambda)\right]^2 d\lambda \tag{B8}$$

By further stipulating a uniform cantilevered beam and using a mode shape $\phi(x)$ which corresponds to that for a concentrated static load at the tip,

$$EI(x) = EI$$

$$\phi(x) = \frac{1}{2L^3}\left(3Lx^2 - x^3\right) \tag{B9}$$

from which is obtained

$$\left.\begin{aligned} M &= m \\ \omega^2 &= \frac{3EI}{mL^3} \\ L\,\Delta(L) &= \frac{6}{5} \end{aligned}\right\} \tag{B10}$$

Substituting equations (B10) into the equation of motion (B7) yields

$$m\ddot{q} + \left[m\left(\omega^2 - \Omega^2\right) + \frac{6m}{5}\Omega^2\right]q = Q(t) \tag{B11}$$

where $\frac{6m}{5}\Omega^2$ is the centrifugal stiffening term. Thus,

$$\ddot{q} + \left(\omega^2 + \frac{1}{5}\Omega^2\right)q = \frac{1}{m}Q(t) \tag{B12}$$

where $Q(t)$ is the generalized force associated with the mode $\phi(x)$ as defined in equations (B4). Equation (B12) is a second-order linear differential equation with constant coefficients. The general solution will depend on the form of $Q(t)$; however, the homogeneous form of the equation is

$$\ddot{q} + \left(\omega^2 + \frac{1}{5}\Omega^2\right)q = 0 \tag{B13}$$

which is oscillatory and has a natural frequency ω_n

$$\omega_n = \omega^2 + \frac{1}{5}\Omega^2 \tag{B14}$$

Thus, the dependence of ω_n on the rotational rate Ω by virtue of the $\frac{1}{5}\Omega^2$ term includes a centrifugal stiffening effect. (See refs. 1, 2, and 3.)

For a beam with a concentrated tip mass, the desired form of equation (B5) becomes

$$a(L,t) = \frac{1}{2}\Delta(L)\, q^2(t) \tag{B15}$$

which describes a parabola with axis on the undeformed beam axis, regardless of the assumed mode shape $\phi(x)$. However, the coefficient of the parabola $\Delta(L)/2$ is related to the assumed mode shape and determines the amount of shortening and hence stiffening that may result. An aspect showing the importance of this shortening or stiffening may be seen in equation (B3) where the motion is unstable when the stiffening is insufficient, that is,

$$\Omega^2 \int_0^L x\, m(x)\, \Delta(x)\, dx < M\Omega^2$$

For the mode shape assumed in equation (B9), the stiffness is adequate and equation (B15) becomes

$$a(L,t) = \frac{3}{5L}q^2(t) \tag{B16}$$

Because the tip motion for the cantilevered beam traverses a parabola which may be represented by a circle for small deflections, an alternate configuration as shown in appendix C was developed.

APPENDIX C

EFFECTIVE HINGE POINT

In appendix B the equation of motion for a rotating cantilever beam was determined in order to assess the centrifugal stiffening effect. In this appendix an alternative rotating system as shown in sketch (b) is analyzed. When this system is made equivalent to the rotating cantilever beam of appendix B, the effective hinge point may be easily defined.

Symbols

k_t	torsion spring simulating beam bending
L	undeformed length of two-link mechanism
m	tip mass
q	lateral displacement coordinate
X,Y	rotating coordinate axes
x	position along X-axis
α	hinge-point location relative to length L
Δ	composite function of length and hinge-point location (see eq. (C5))
θ	coordinate of rotation about hinge point
Ω	rotational speed
ω	uncoupled natural frequency about hinge point (see eq. (C4))

Dots over symbols denote time derivatives.

Analysis of Rotating System

Consider the two-link rotating system shown in sketch (b). The system is constrained to rotate uniformly at a constant rate Ω. Coupling of the two links is provided

APPENDIX C

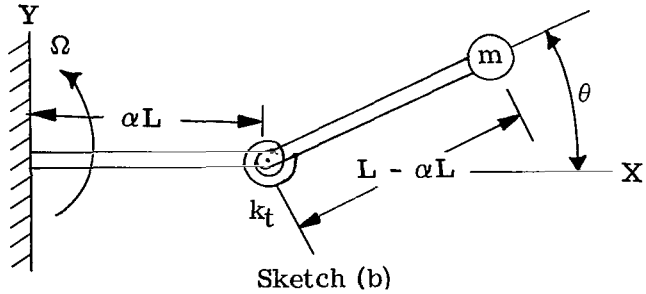

Sketch (b)

by means of a torsional spring of stiffness k_t. At any time, the deflection of the mass m from the X-axis may be determined in terms of θ. The net movement of m, it should be noted, consists of a motion transverse to the X-axis and a motion along the X-axis. If the equation of motion for the system is derived and then linearized by using a small angle assumption on θ ($\sin\theta \approx \theta$), the resulting equation is:

$$m(L - \alpha L)^2\ddot{\theta} + m\alpha L\Omega^2(L - \alpha L)\theta + k_t\theta = 0 \tag{C1}$$

If the lateral deflection is defined as

$$\dot{q} = (L - \alpha L)\theta \tag{C2}$$

then equation (C1) may be written as

$$\ddot{q} + \left(\omega^2 + \frac{\alpha L\Omega^2}{L - \alpha L}\right)q = 0 \tag{C3}$$

where the substitution

$$\omega^2 = \frac{k_t}{m(L - \alpha L)^2} \tag{C4}$$

has been made.

Comparing equations (C3) and (B7) for unforced motion and defining $\Delta \equiv \Delta(L)$ gives

$$\Delta = \frac{1}{L - \alpha L} \tag{C5}$$

or

$$\alpha = \frac{L\Delta - 1}{L\Delta} \tag{C6}$$

where $0 \leqq \alpha \leqq 1$ and αL locates an effective hinge point as measured from the actual center of rotation (x = 0). Thus, equation (C6) defines the normalized position of a center about which the tip of a beam effectively pivots during small deflections.

REFERENCES

1. Den Hartog, J. P.: Mechanical Vibrations. Fourth ed., McGraw-Hill Book Co., Inc., 1956.

2. Coleman, Robert P.; and Feingold, Arnold M.: Theory of Self-Excited Mechanical Oscillations of Helicopter Rotors With Hinged Blades. NACA Rep. 1351, 1958. (Supersedes NACA TN 3844.)

3. Brooks, George W.: The Mechanical Instability and Forced Response of Rotors on Multiple-Degree-of-Freedom Supports. Ph.D. Thesis, Princeton Univ., 1961.

4. Bisplinghoff, Raymond L.; Ashley, Holt; and Halfman, Robert L.: Aeroelasticity. Addison-Wesley Pub. Co., Inc., c.1955.

5. Herrmann, G.; and Bungay, R. W.: On the Stability of Elastic Systems Subjected to Nonconservative Forces. Trans. ASME, Ser. E: J. Appl. Mech., vol. 31, no. 3, Sept. 1964, pp. 435-440.

6. Sleeper, R. K.; and Lester, H. C.: A Dynamic Stability Study of a Centrifuge-Equipped Space Station. J. Spacecraft and Rockets, vol. 5, no. 12, Dec. 1968, pp. 1432-1437.

7. Hurty, Walter C.; and Rubinstein, Moshe F.: Dynamics of Structures. Prentice-Hall Inc., c.1964.

8. Foss, Kenneth A.: Coordinates Which Uncouple the Equations of Motion of Damped Linear Dynamic Systems. Tech. Rep. 25-20 (Contract N5ori-07833), M.I.T., Mar. 1956.

9. Fuller, A. T.: Stability Criteria for Linear Systems and Realizability Criteria for RC Networks. Proc. Cambridge Phil. Soc., vol. 53, pt. 4, Oct. 1957, pp. 878-896.

10. Chestnut, Harold; and Mayer, Robert W.: Servomechanisms and Regulating System Design. Vol. I. Second ed., John Wiley & Sons, Inc., c.1959.

11. Ogata, Katsuhiko: State Space Analysis of Control Systems. Prentice-Hall, Inc., c.1967.

12. Zadeh, Lotfi A.; and Desoer, Charles A.: Linear System Theory – The State Space Approach. McGraw-Hill Book Co., Inc., c.1963.

13. Herrmann, G.; and Jong, Ing-Chang: On the Destabilizing Effect of Damping in Nonconservative Elastic Systems. Trans. ASME, Ser. E: J. Appl. Mech., vol. 32, no. 3, Sept. 1965, pp. 592-597.

14. Den Hartog, J. P.: Advanced Strength of Materials. McGraw-Hill Book Co., Inc., 1952.

15. Lanczos, Cornelius: The Variational Principles of Mechanics. Second ed., Univ. of Toronto Press, c.1962.

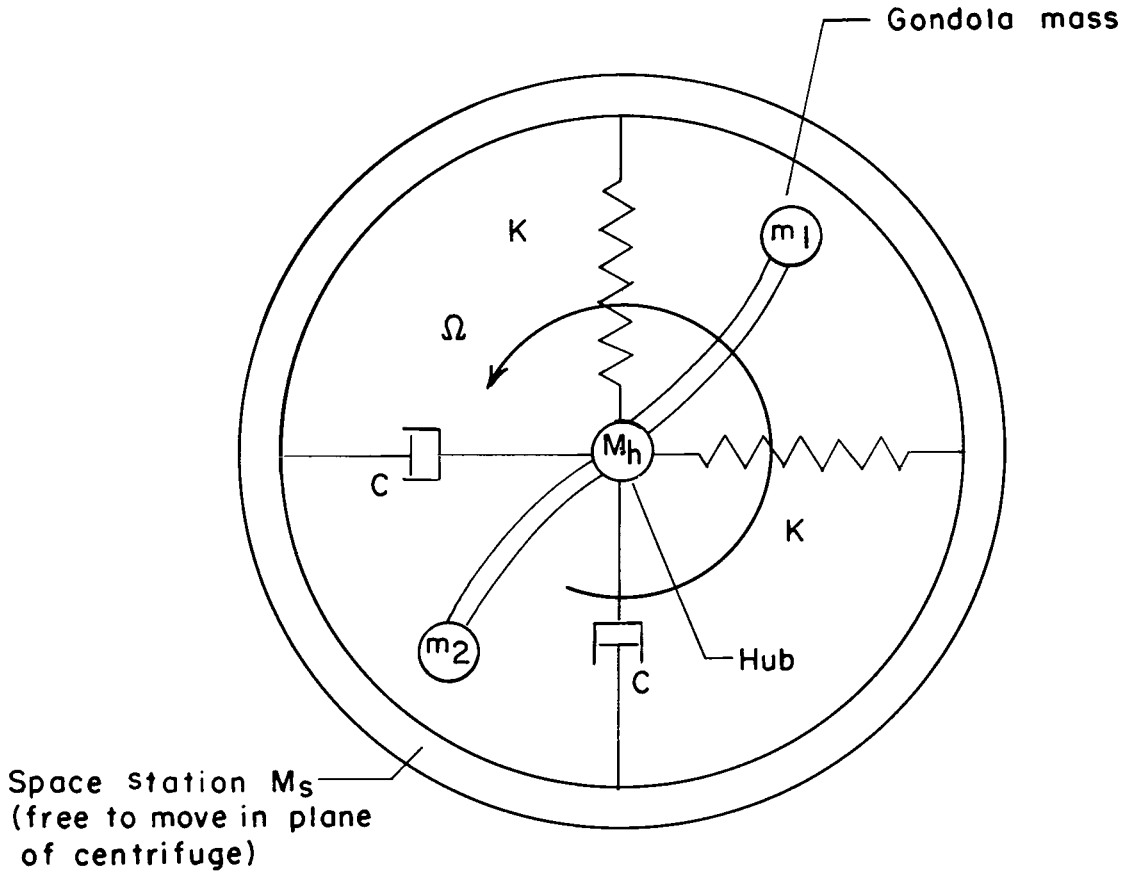

Figure 1.- Space-station—centrifuge model.

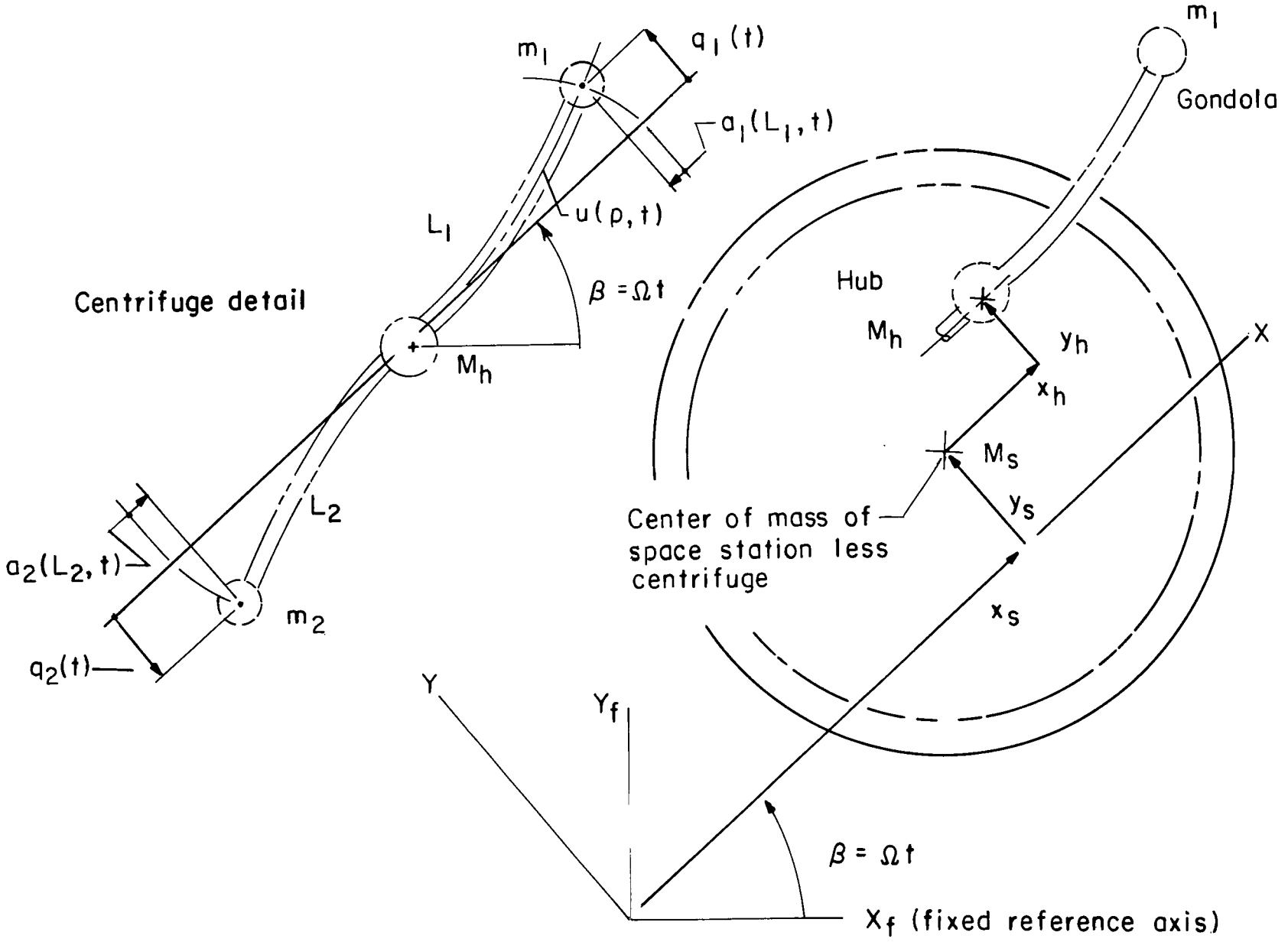

Figure 2.- Rotating coordinate system.

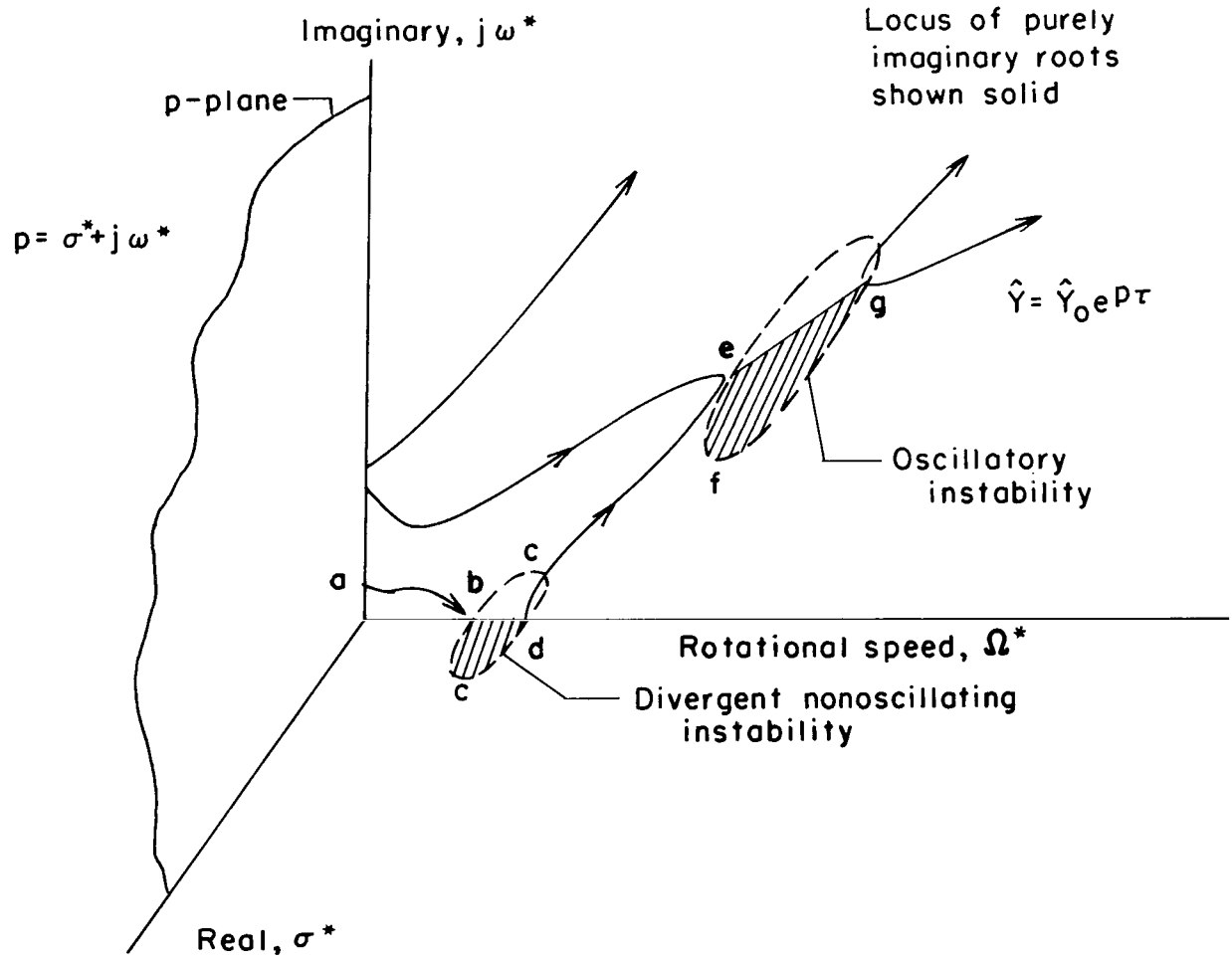

Figure 3.- Typical upper half of root locus for rotating system. Surfaces described by roots with positive real parts ($\sigma > 0$) are shown hatched.

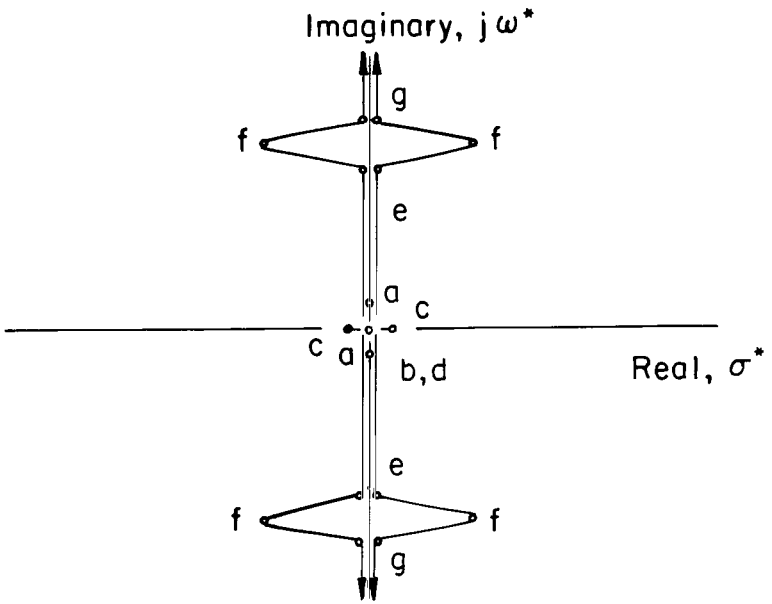

(a) p-plane, $p = \sigma^* + j\omega^*$. Instability exhibited by departure of roots from imaginary axis of p-plane into right half-plane.

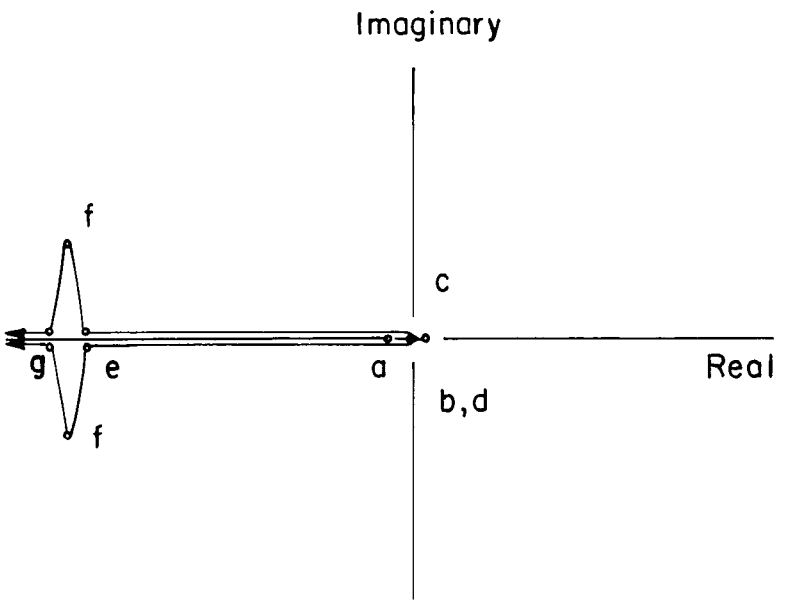

(b) p^2-plane. Instability exhibited by departure of roots from negative real axis of p^2-plane.

Figure 4.- Locus of roots as function of rotational speed for even stability polynomial in p-plane and p^2-plane. Rotational speeds Ω^* increase from 0 for a through g.

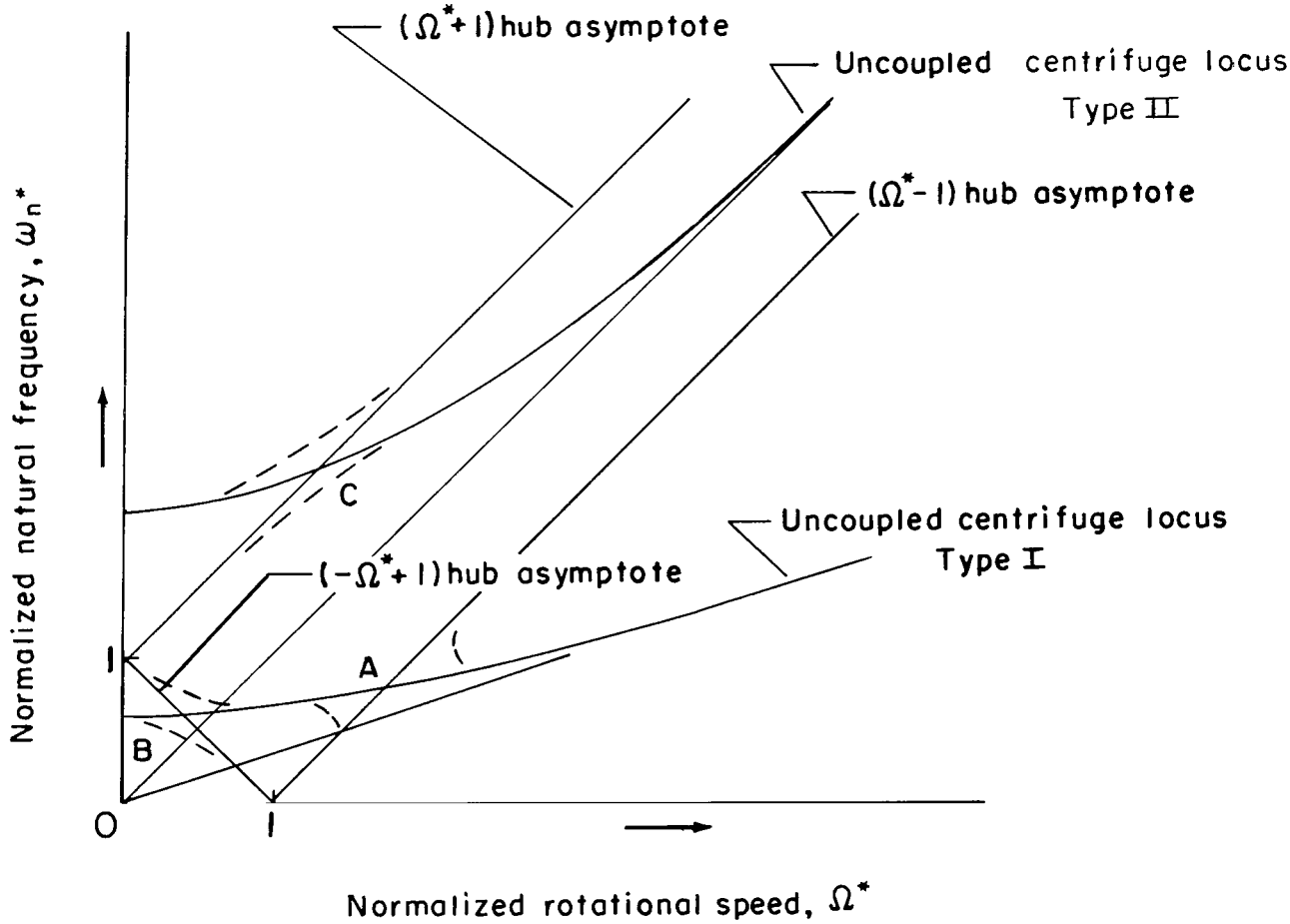

Figure 5.- Uncoupled loci of stability determinant.

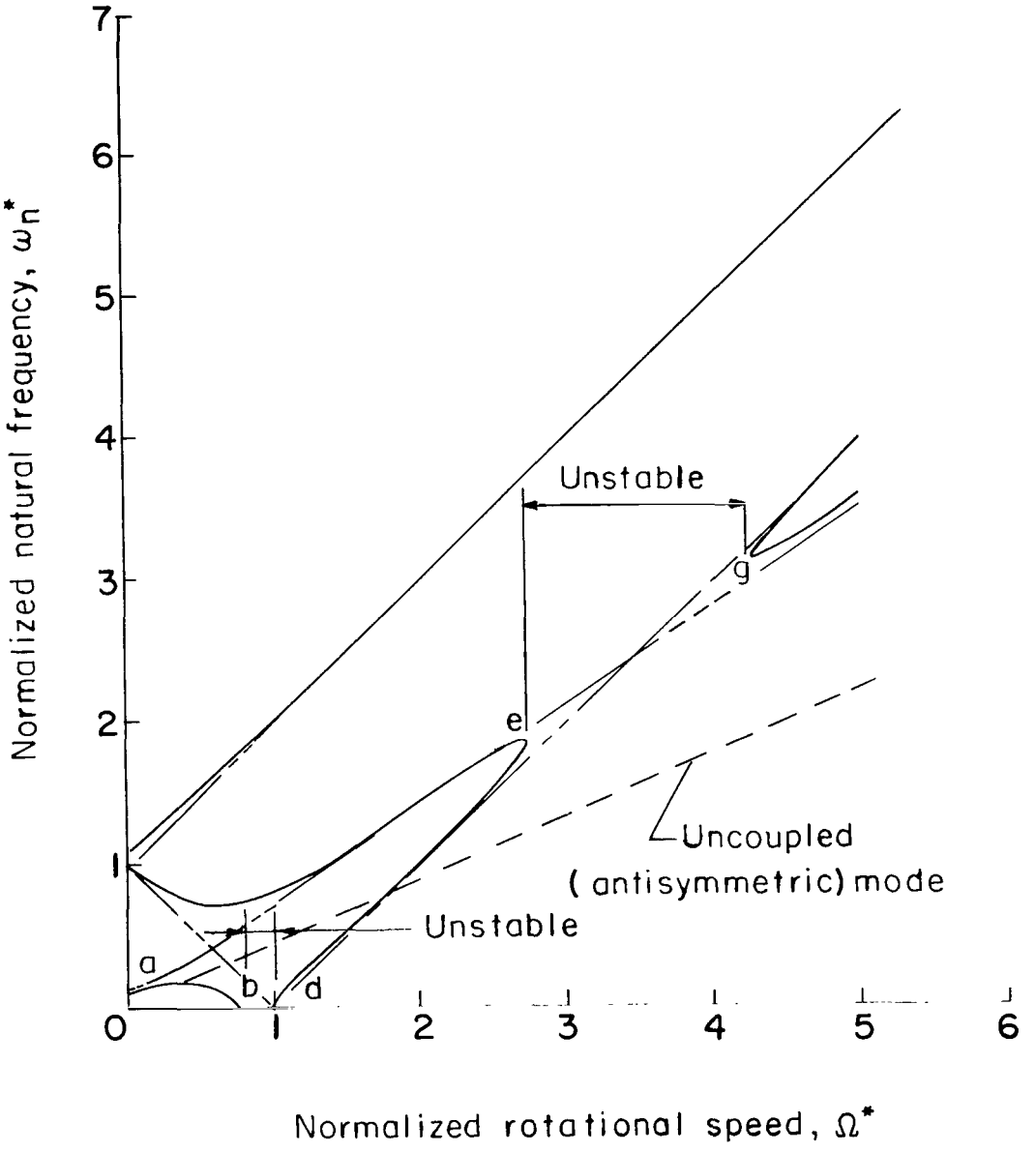

Figure 6.- Natural frequencies of basic model in rotating reference frame. $\mu_1 = \mu_2 = 0.1$, $\mu_3 = 0.01$, $\omega_1^* = \omega_2^* = 0.1$, and $\alpha_1 = \alpha_2 = 1/6$. Asymptotes shown in phantom.

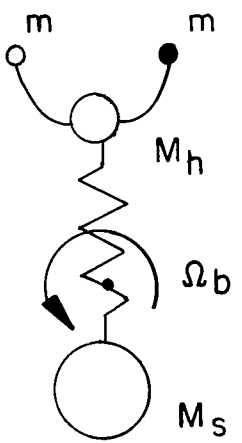

Gondola masses
deflect equally

$q_1 = q_2 =$ Constant

(a) Lower critical-speed mode.

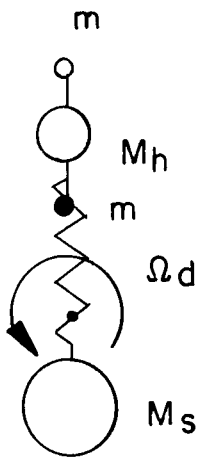

Gondola masses
do not deflect

$q_1 = q_2 = 0$

(b) Upper critical-speed mode.

Figure 7.- Upper and lower critical-speed modes. $m_1 = m_2 = m$.

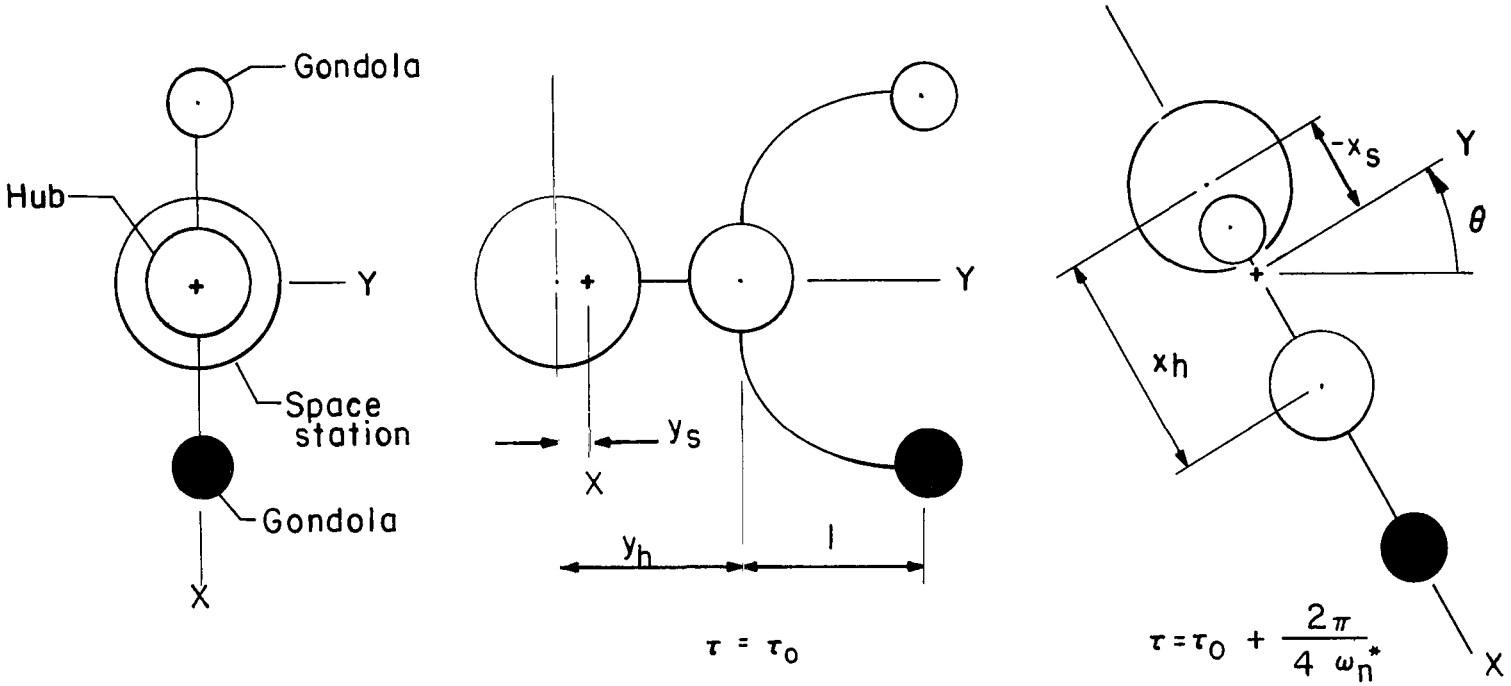

(a) Undeformed position.

(b) Deformed position.

Figure 8.- Typical mode shape as seen by observer in the fixed reference frame. + denotes center of mass of system.

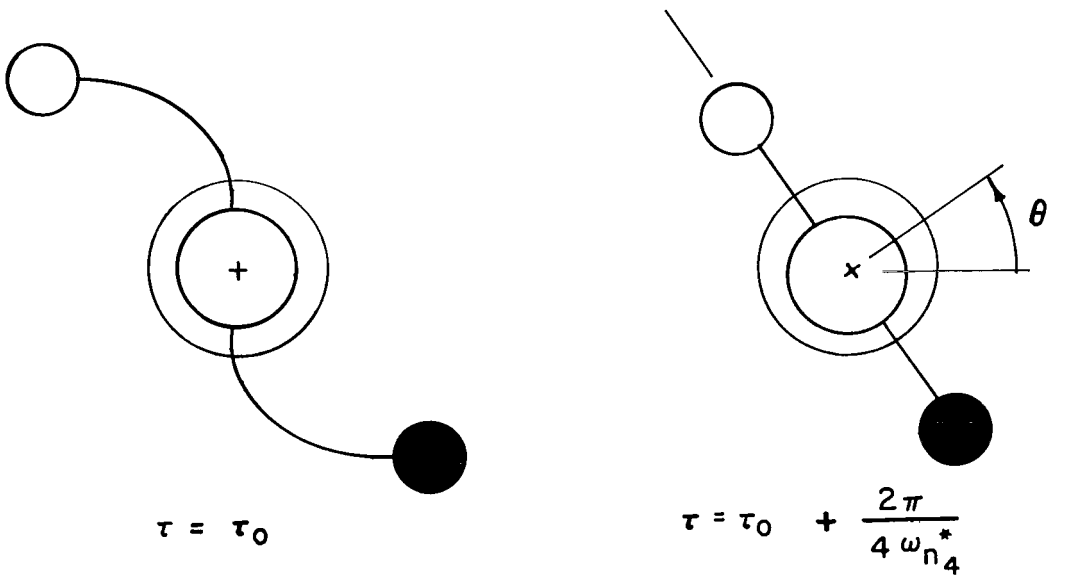

Figure 9.- Uncoupled antisymmetric mode shape of symmetric configuration.

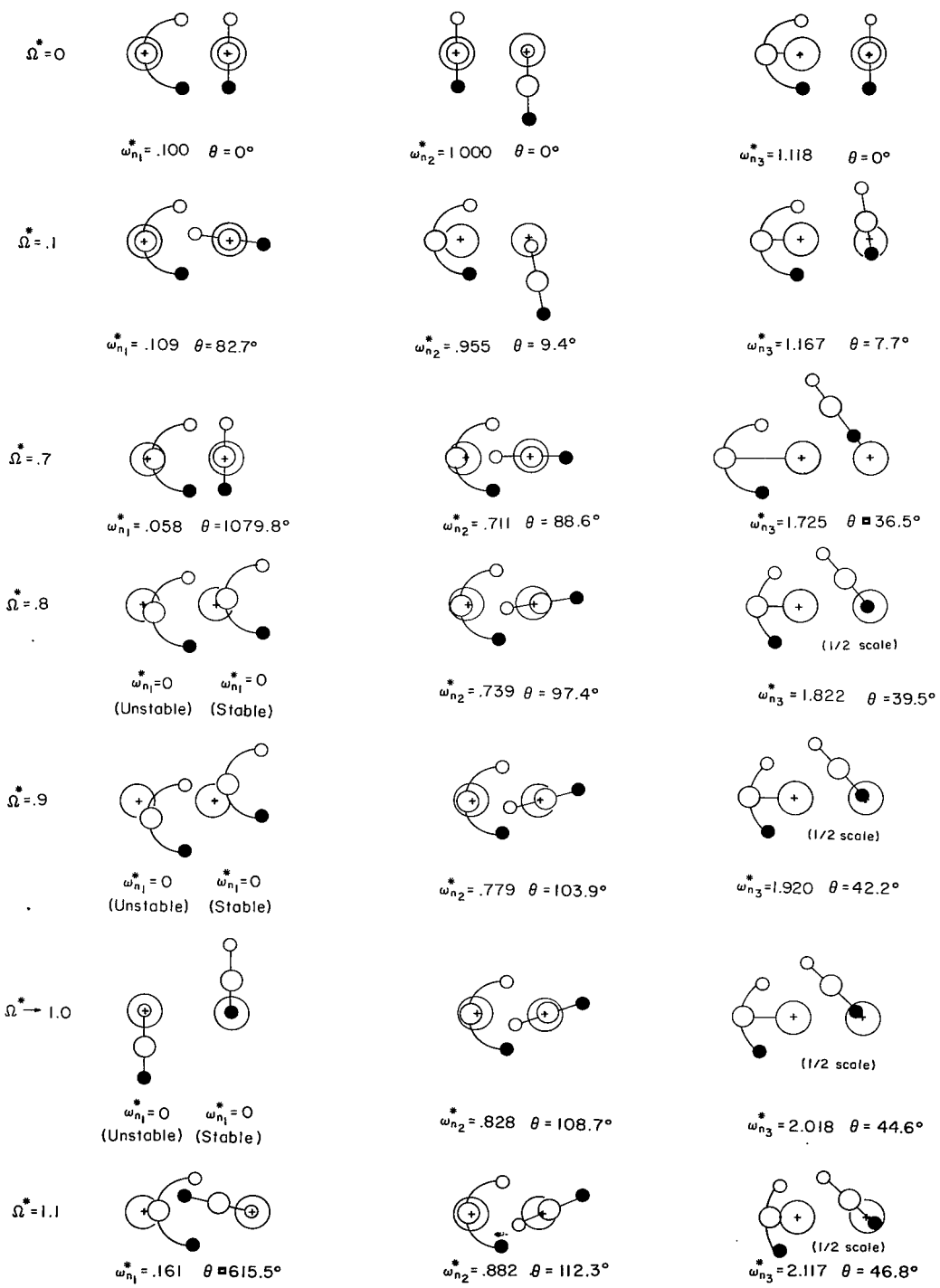

Figure 10.- Typical mode shapes for symmetric undamped model with oscillatory instability.

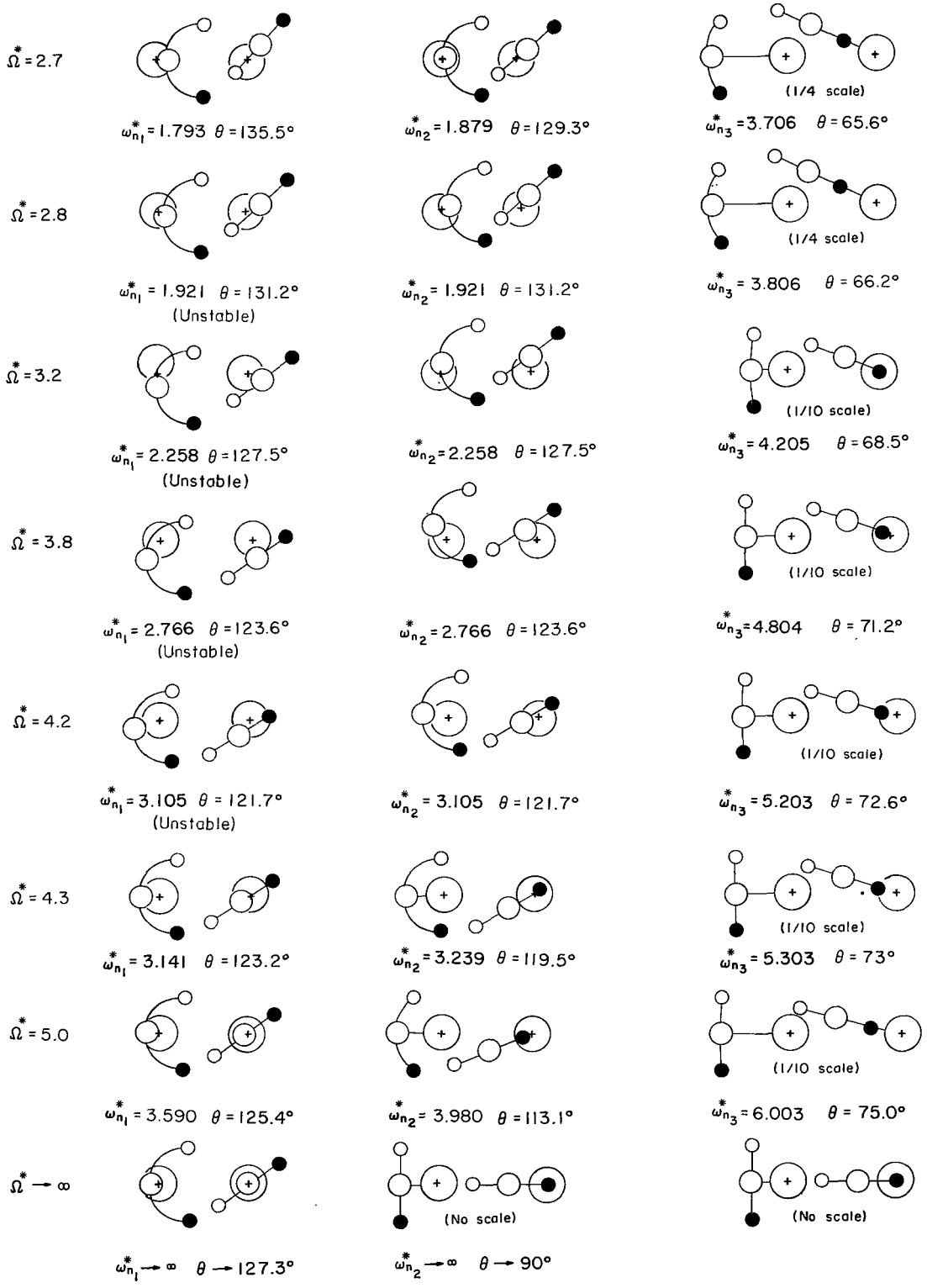

Figure 10.- Concluded.

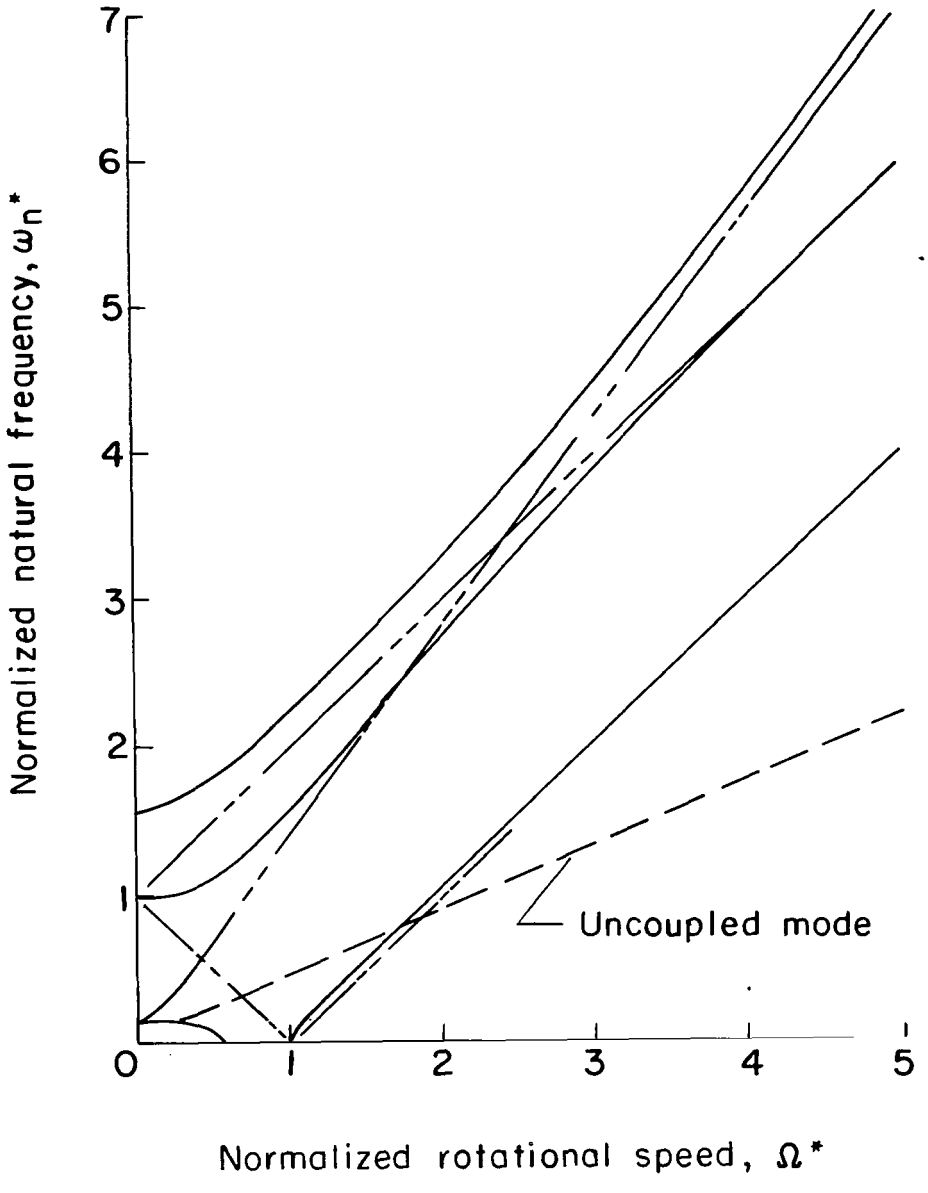

Figure 11.- Natural frequencies in rotating frame with $\mu_1 = \mu_2 = 0.3$, $\mu_3 = 0.01$, $\omega_1^* = \omega_2^* = 0.1$ and $\alpha_1 = \alpha_2 = 1/6$. Asymptotes shown in phantom.

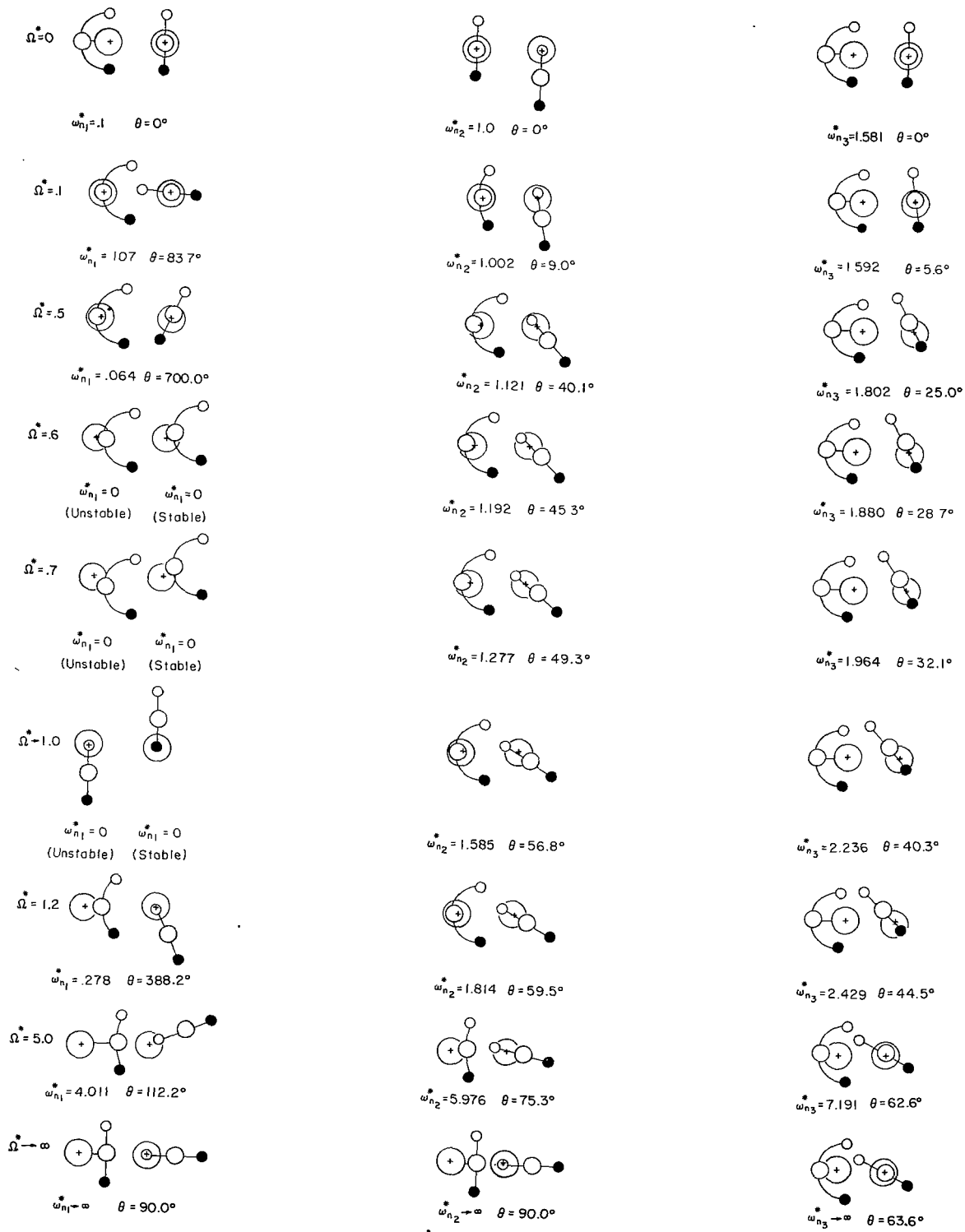

Figure 12.- Typical mode shapes for symmetric undamped model without oscillatory instability.

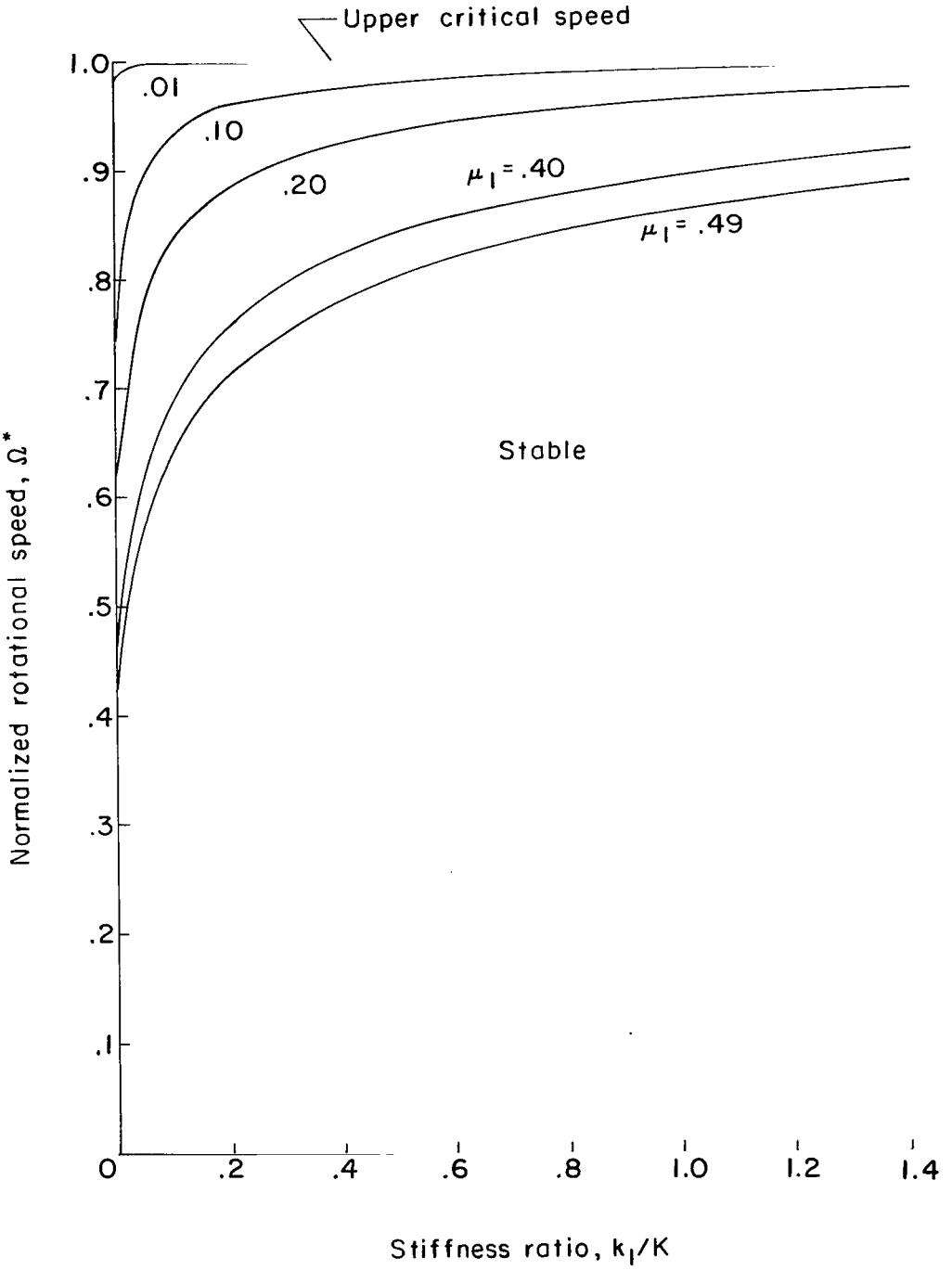

(a) Critical-speed regions.

Figure 13.- Instability regions for symmetrical undamped model with $\mu_3 = 0.01$ and $\alpha_1 = \alpha_2 = 1/6$.

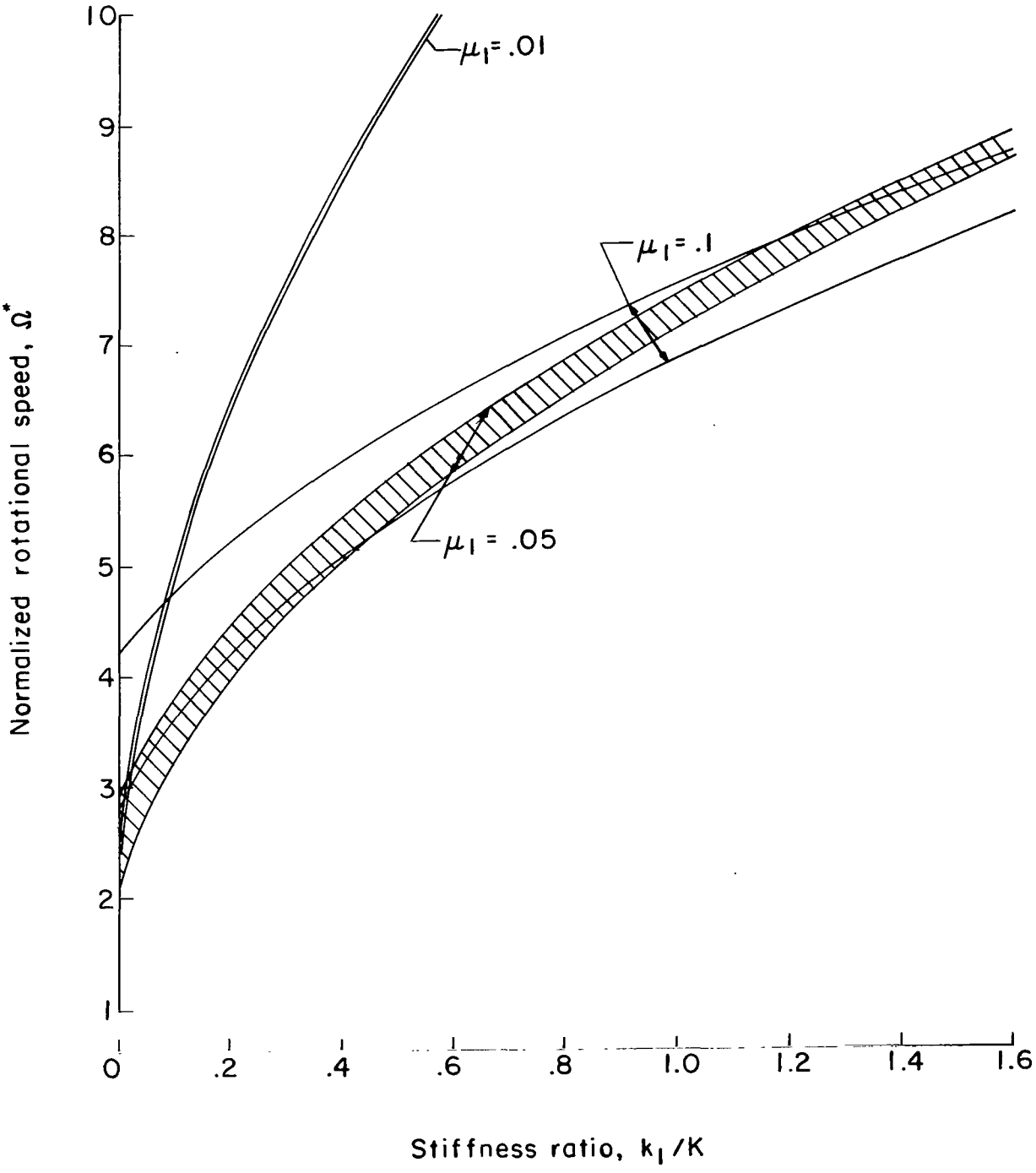

(b) Oscillatory divergent instability regions. No mechanical instabilities exist for $\mu_1 \geq 0.2$.

Figure 13.- Concluded.

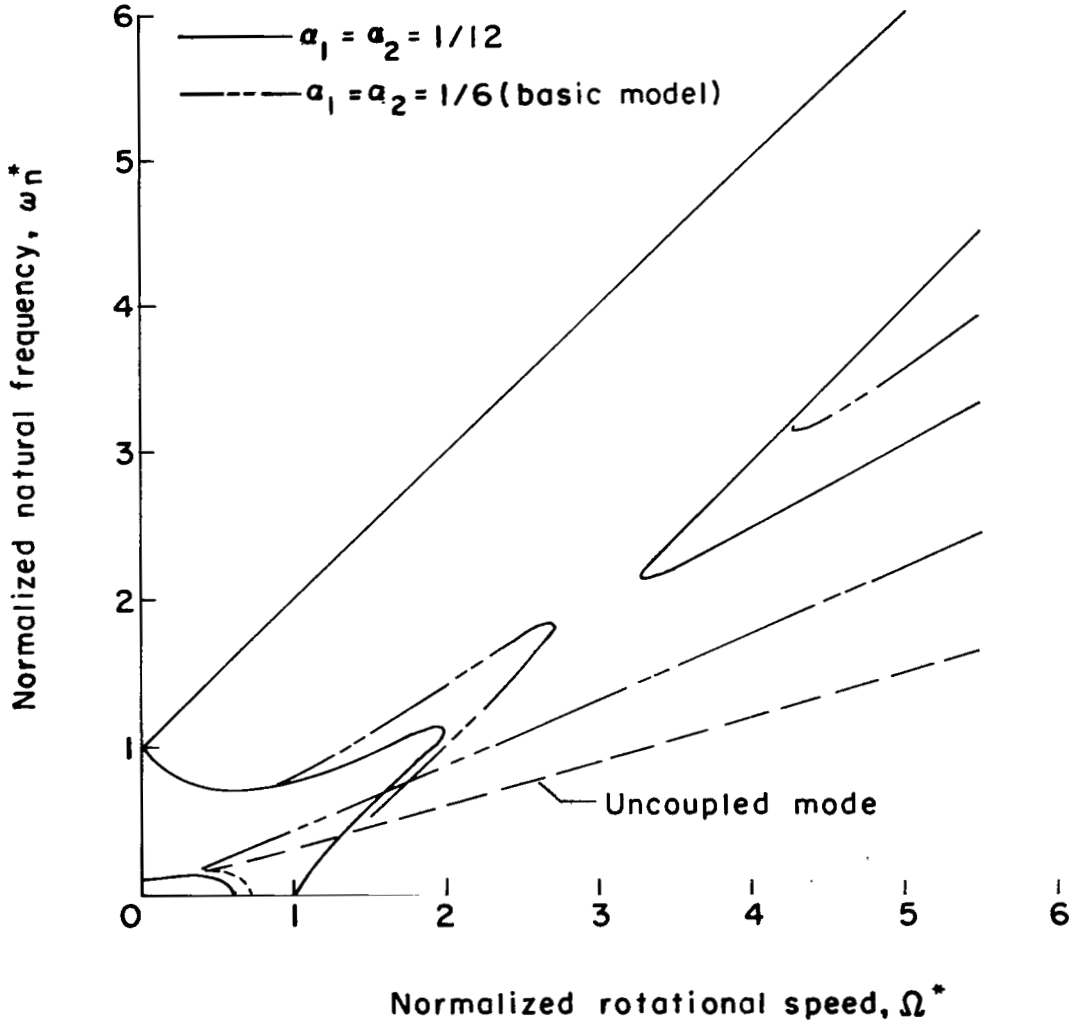

Figure 14.- Result of inboard effective hinge location on natural frequencies in rotating reference frame. $\mu_1 = \mu_2 = 0.1$, $\mu_3 = 0.01$, and $\omega_1^* = \omega_2^* = 0.1$.

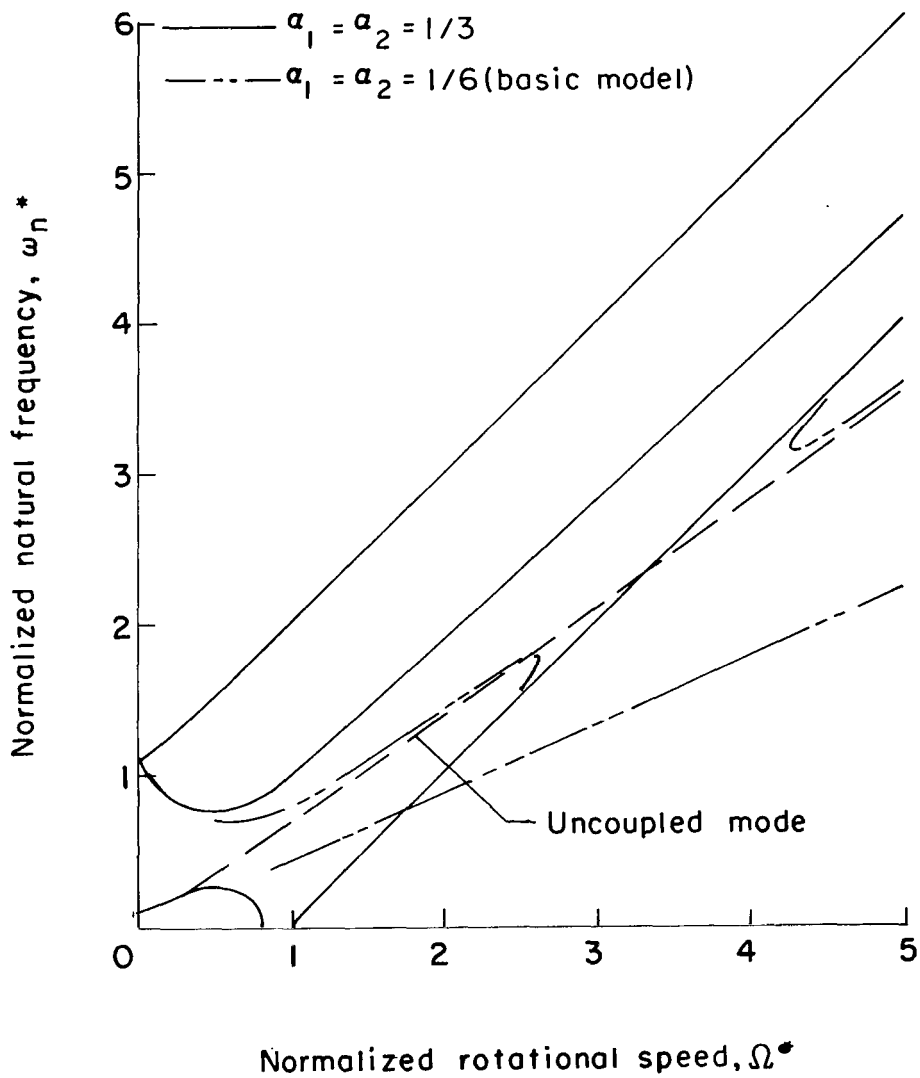

Figure 15.- Result of outboard effective hinge location on natural frequencies in rotating reference frame. $\mu_1 = \mu_2 = 0.1$, $\mu_3 = 0.01$, and $\omega_1^* = \omega_2^* = 0.1$.

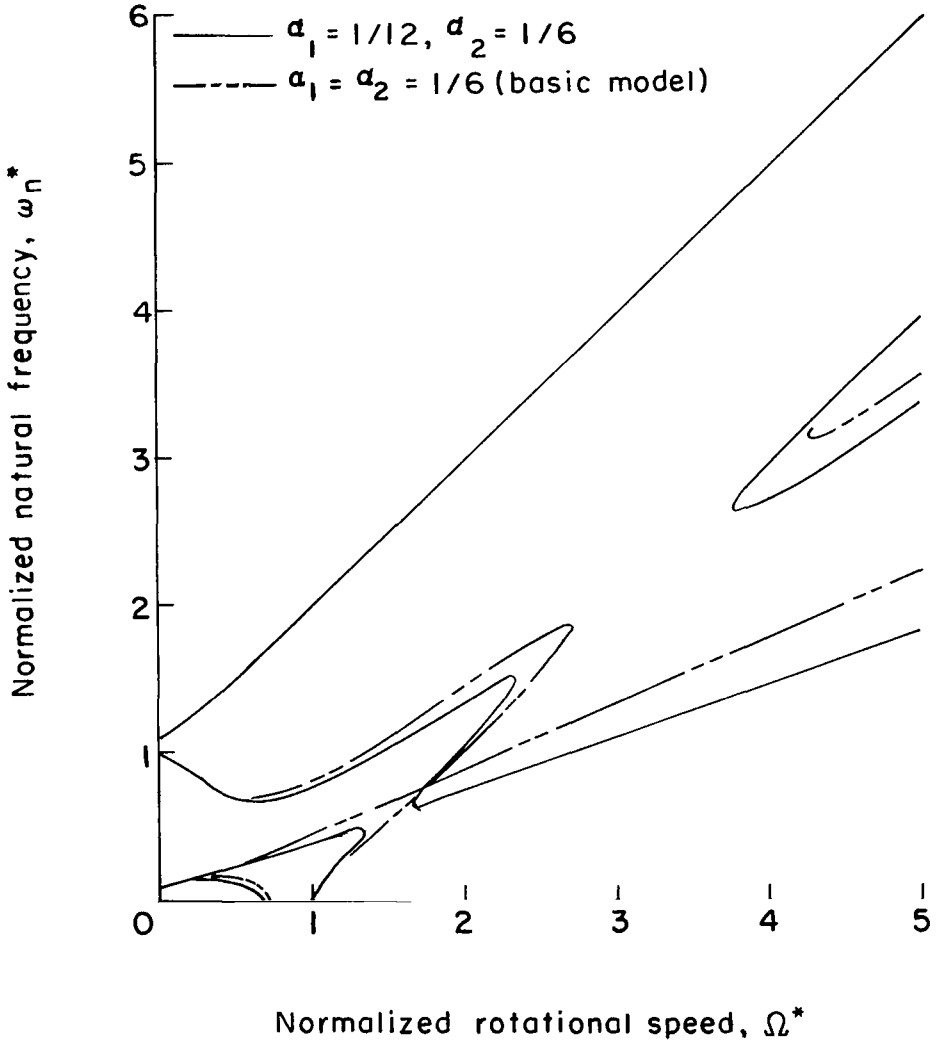

Figure 16.- Result of nonsymmetrical effective hinge-point location on natural frequencies in rotating reference frame. $\mu_1 = \mu_2 = 0.1$, $\mu_3 = 0.01$, and $\omega_1^* = \omega_2^* = 0.1$.

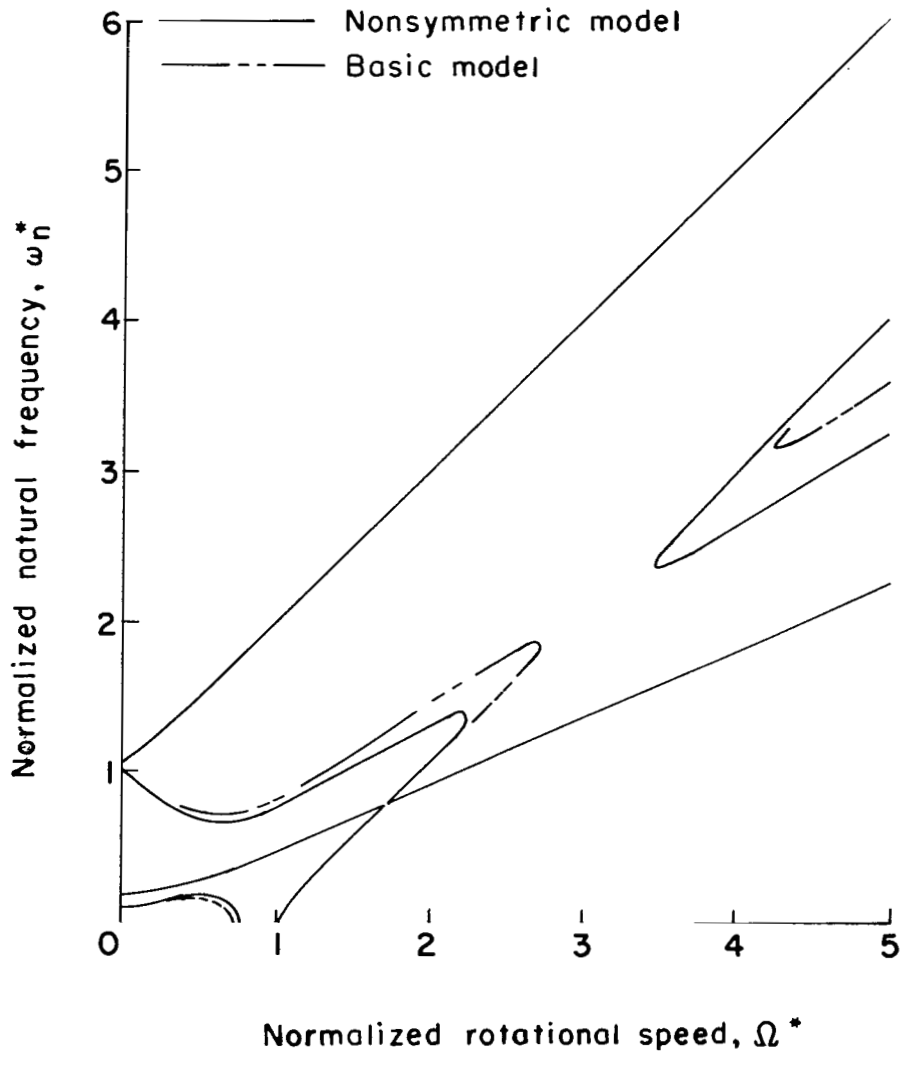

Figure 17.- Result of a balanced nonsymmetrical centrifuge on natural frequencies in rotating reference frame. $\mu_1 = 0.05$, $\mu_2 = 0.1$, $\mu_3 = 0.01$, $\omega_1^* = 0.1$, $\omega_2^* = 0.2$, and $\alpha_1 = \alpha_2 = 1/6$.

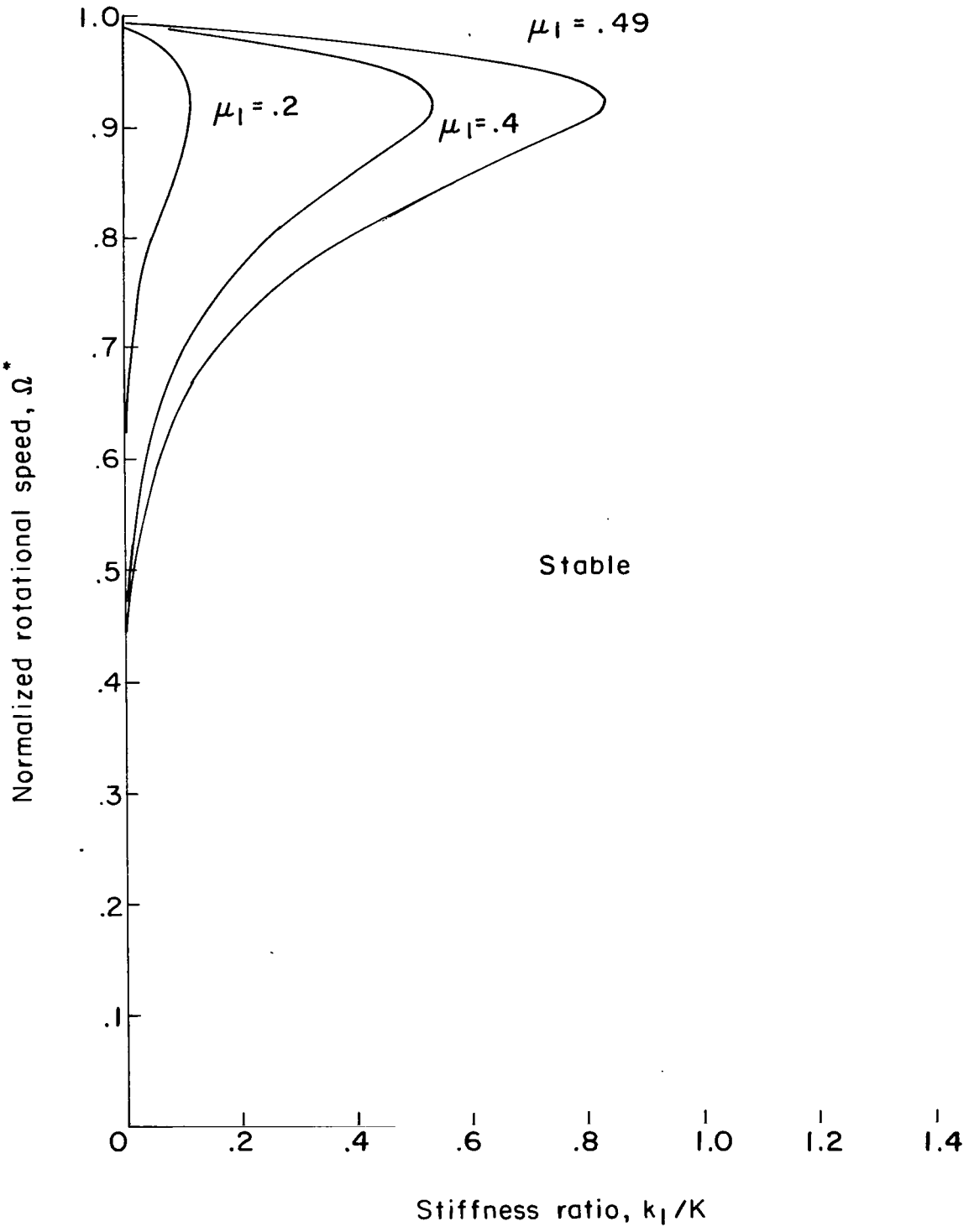

Figure 18.- Effect of support structure damping on critical-speed instability regions. $\mu_3 = 0.01$, $\alpha_1 = \alpha_2 = 1/6$, $\zeta_1 = \zeta_2 = 0.01$, and $\zeta = 0.1$.

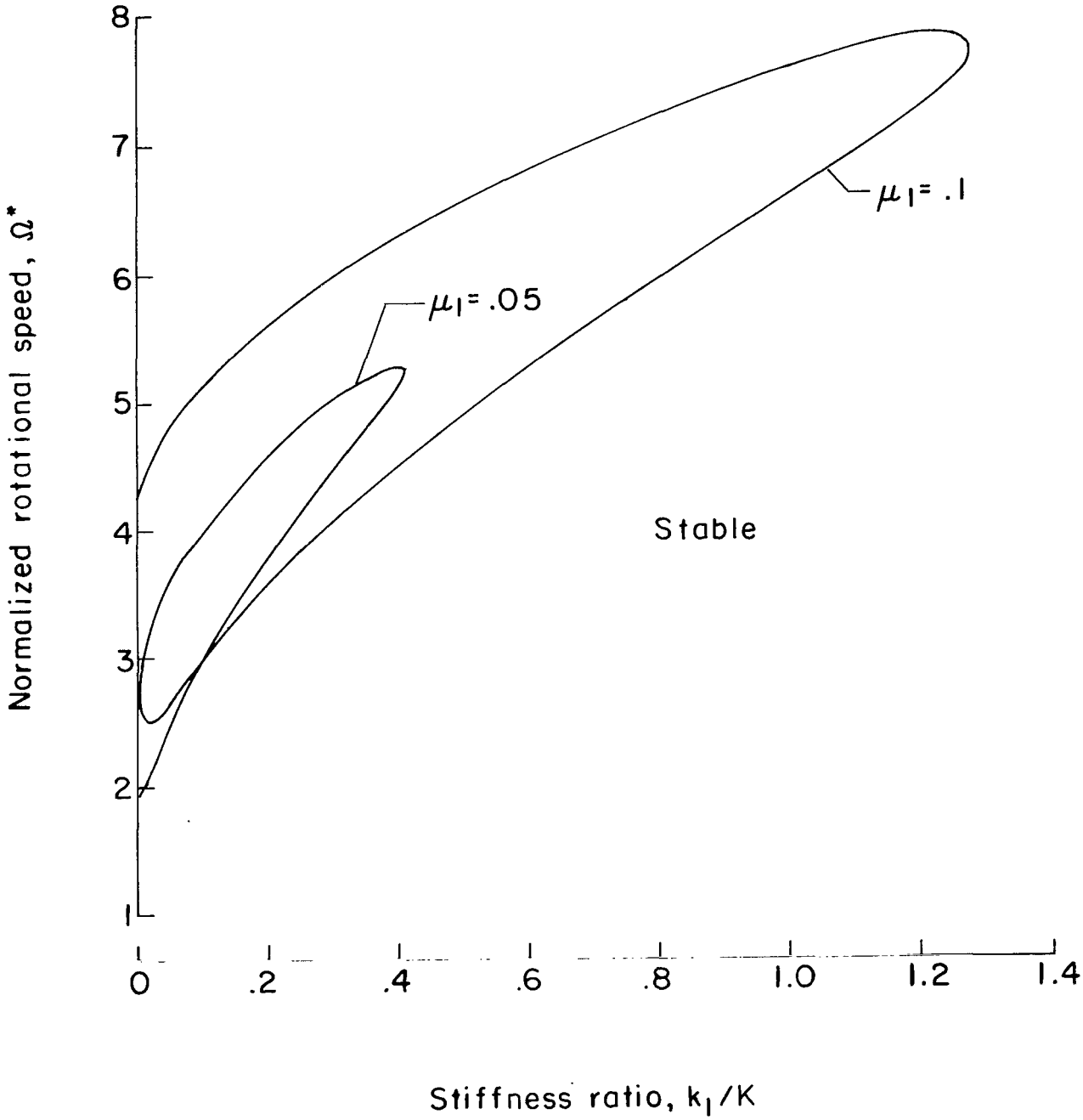

Figure 19.- Effect of moderate centrifuge arm damping on the oscillatory divergent instability regions. $\mu_3 = 0.01$, $\alpha_1 = \alpha_2 = 1/6$, $\zeta_1 = \zeta_2 = 0.1$, and $\zeta = 0.01$.

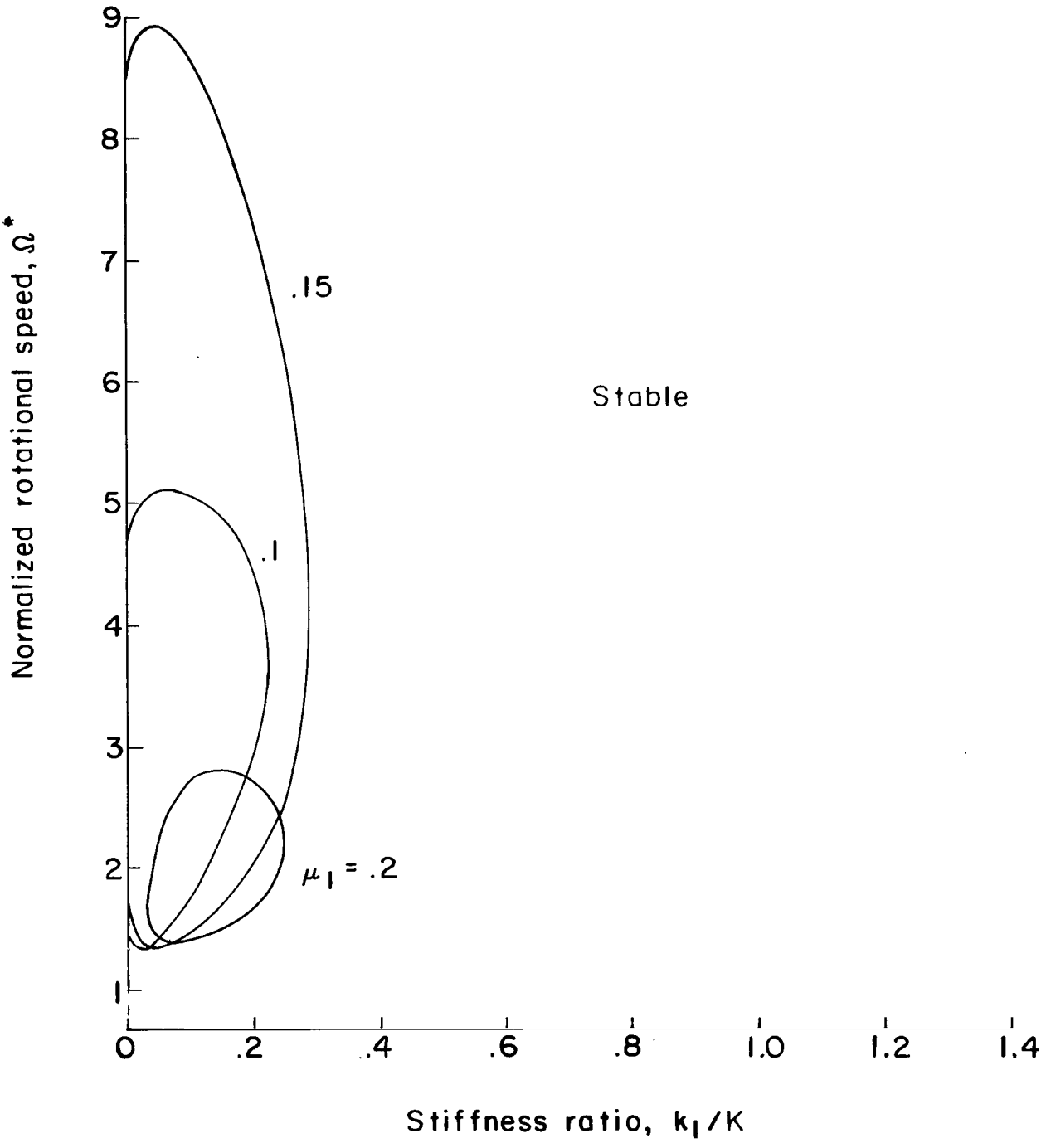

Figure 20.- Effect of heavy centrifuge arm damping on the oscillatory divergent instability regions. $\mu_3 = 0.01$, $\alpha_1 = \alpha_2 = 1/6$, $\zeta_1 = \zeta_2 = 0.5$, and $\zeta = 0.01$.

NATIONAL AERONAUTICS AND SPACE ADMINISTRATION
WASHINGTON, D. C. 20546

OFFICIAL BUSINESS

FIRST CLASS MAIL

POSTAGE AND FEES PAID
NATIONAL AERONAUTICS AND
SPACE ADMINISTRATION

"The aeronautical and space activities of the United States shall be conducted so as to contribute . . . to the expansion of human knowledge of phenomena in the atmosphere and space. The Administration shall provide for the widest practicable and appropriate dissemination of information concerning its activities and the results thereof."

—NATIONAL AERONAUTICS AND SPACE ACT OF 1958

NASA SCIENTIFIC AND TECHNICAL PUBLICATIONS

TECHNICAL REPORTS: Scientific and technical information considered important, complete, and a lasting contribution to existing knowledge.

TECHNICAL NOTES: Information less broad in scope but nevertheless of importance as a contribution to existing knowledge.

TECHNICAL MEMORANDUMS: Information receiving limited distribution because of preliminary data, security classification, or other reasons.

CONTRACTOR REPORTS: Scientific and technical information generated under a NASA contract or grant and considered an important contribution to existing knowledge.

TECHNICAL TRANSLATIONS: Information published in a foreign language considered to merit NASA distribution in English.

SPECIAL PUBLICATIONS: Information derived from or of value to NASA activities. Publications include conference proceedings, monographs, data compilations, handbooks, sourcebooks, and special bibliographies.

TECHNOLOGY UTILIZATION PUBLICATIONS: Information on technology used by NASA that may be of particular interest in commercial and other non-aerospace applications. Publications include Tech Briefs, Technology Utilization Reports and Notes, and Technology Surveys.

Details on the availability of these publications may be obtained from:

SCIENTIFIC AND TECHNICAL INFORMATION DIVISION

NATIONAL AERONAUTICS AND SPACE ADMINISTRATION

Washington, D.C. 20546